ADVANCED MASTERS IN STRUCTURAL ANALYSIS
OF MONUMENTS AND HISTORICAL CONSTRUCTIONS

Master's Thesis

Benjamin Forrest

Simulation of Masonry Arch Experimentation using 3D Finite Element Analysis

This Masters Course has been funded with support from the European Commission. This publication reflects the views only of the author, and the Commission cannot be held responsible for any use which may be made of the information contained therein.

Barcelona | 2012

DECLARATION

Name: Benjamin Forrest

Email: forrestbt@gmail.com

Title of the Msc Dissertation: Simulation of Masonry Arch Experiments using 3D Finite Element Analysis

Supervisor(s): Climent Molins

Year: 2012

I hereby declare that all information in this document has been obtained and presented in accordance with academic rules and ethical conduct. I also declare that, as required by these rules and conduct, I have fully cited and referenced all material and results that are not original to this work.

I hereby declare that the MSc Consortium responsible for the Advanced Masters in Structural Analysis of Monuments and Historical Constructions is allowed to store and make available electronically the present MSc Dissertation.

University: UPC

Date: 16 July 2012

Signature: _____

ACKNOWLEDGEMENTS

There are several parties which contributed to the completion of this work. In particular I would like to thank:

My supervisor and mentor, Professor Climent Molins: Throughout my research, he has been a source of knowledge and support towards the completion of this dissertation.

Tasos Drougkas and Oriol Arneau: Their useful advice and knowledge, specifically when dealing with the FE program and understanding the significance of the results has led me to this success.

The Erasmus Mundus Committee and European Union: Their financial support and organization of this program enabled my Master's study abroad.

I would also like to make a special acknowledgement to the members of my family:

My father, Thorne Forrest: He has been a never ending source of encouragement and support throughout the completion of this dissertation.

My mother, Lucille Forrest: She was always present to offer advice or encouragement throughout writing of this dissertation.

Finally, all the other family members and friends who encouraged me to participate in the program and have provided me with support ever since.

ABSTRACT

In the design world, there exists two spaces. One space is the physical domain, and the other, the numerical domain. Researchers, engineers and mathematicians alike have all been trying to bridge the gap between these two domains. In the case of the engineering field, this motivation is driven by the requirement to understand the exact responses of a structure so they can be confident their designs will succeed. The Finite Element Method is a huge leap in goal of bridging these two domains together. Since its implementation in the study of structural responses, electromagnetic fields and flow theory, several analysts and researchers have come up with new innovations in order to improve the method and have the numerical results approach the realistic responses.

This dissertation is a study to determine how close an experiment on a scale model masonry bridge can be simulated. A scale model segmental arch bridge (3.2m span, 1 m thick) was loaded until failure in the structural laboratory at the Universitat de Politecnica de Catalunya in 2001. The results of the experiment were recorded and were used as a source of comparison for models generated with finite element software.

Originally this dissertation was too being a continuation of a previous dissertation done on the same experiment. However, the models were not able to be verified so it became necessary to generate new models. For generation of the new models, an innovative interface insertion technique was applied to ensure the correct implementation of the interface elements.

The 3D model was completed in stages. At each stage, the results were compared with both those of the previous dissertation and the experimental data. Once the results were verified, the next model was generated. The first model was a plane stress model fully supported with only one layer of soil. The second model incorporated five layers of soil and a steel wall and tie lateral constraint system. The third model was a 3D model of half of the actual bridge (one symmetrical half).

The first two models yielded acceptable results when compared to the previous models and the experimental data. The third model, however, did not possess the expected structural responses. This is attributed to the complex nature of modeling 3D structures due to the multitude of variables involved. Due to obtaining acceptable results from the predecessor models, it is possible that with continued work on the 3D model, it will yield acceptable results as well. It will be a matter of manipulating variables such as the nonlinear properties of the masonry and of the interfaces.

RESUM

En el món del disseny, hi ha dos espais. Un espai és el domini físic, i l'altre, el domini numèric. Els investigadors, enginyers i matemàtics per igual han estat tractant de tancar la bretxa entre aquests dos dominis. En el cas de la camp de l'enginyeria, aquesta motivació està impulsada pel requisit d'entendre les respostes exactes d'una estructura de manera que es pugui estar segur que seus dissenys tindran èxit. El mètode d'elements finits és un gran salt en la meta de superar aquests dos dominis conjuntament. Des de la seva implementació en l'estudi de les respostes estructurals, els camps electromagnètics i la teoria del flux, diversos analistes i investigadors han arribat amb noves innovacions per tal de millorar el mètode i que els resultats numèrics d'apropar-se les respostes realistes.

Aquesta tesi és un estudi per determinar fins a quin punt es pot simular un assaig d'un pont de maçoneria a escala. Un model a escala de pont d'arc, de 3,2 m de llum i 1 m d'amplària, es va carregar fins a la fallada estructural al laboratori de la Universitat de Politècnica de Catalunya l'any 2001. Els resultats de l'experiment es van registrar i es van utilitzar com una font de comparació per als models generats amb el programari d'elements finits.

Originalment aquesta tesi havia ser una continuació d'una tesi realitzada anteriorment sobre el mateix experiment. No obstant això, els models de què es disposava eren insuficients i va ser necessari per generar nous models. Per a la generació dels nous models, es va aplicar una tècnica innovadora d'inserció dels elements d'interfície per garantir-ne la seva correcta aplicació.

El model 3D es va completar en diverses etapes. En cada etapa, els resultats es van comparar tant amb els de les tesis prèvies com amb les dades experimentals. El primer model va ser un model de tensió plana amb una sol estrat de reble. El segon model va incorporar cinc capes de terra i la placa d'acer com a tap en els extrems. El tercer model és un model 3D de la meitat del pont real (gràcies a la simetria de la càrrega i de l'estructura).

Els dos primers models van donar resultats acceptables comparats amb els models anteriors i les dades experimentals. El tercer model, però, no va presentar les respostes estructurals esperades. Això s'atribueix a la naturalesa complexa de les estructures i del modelatge en 3D, a causa de la multitud de variables que intervenen. A causa de l'obtenció de resultats acceptables dels models anteriors, és probable que amb un treball continu sobre el model 3D, s'abastin resultats acceptables, tot analitzant la influència de les variables, com les propietats no lineals de la maçoneria i de les interfícies.

Contents

1. INTRODUCTION

The evolution of structural analysis has been an ongoing process for a long time. Until the 20th century, structures were analysed and designed using a graphical approach using an equilibrium model of the external forces. The theory of elasticity was born which enabled designers to evaluate both ultimate and service limit states. It wasn't until the middle of the 20th century that the first concepts of, what would become known as finite element analysis, surfaced. The finite element method (FEM) was first implemented in major industries such as aeronautics, automotive and military equipment. It used to be FEM was limited to these large industries because of the requirement for supercomputers to complete the numerical calculations, Now with the advancement in computer technology, practically every personal computer is capable of processing the required calculations. This led to the migration of FEM into the private sector. FEM is now widely used in design in structural analysis, electromagnetism and flow analysis. As FEM became more popular, so too did its infrastructure. Researchers began developing new innovative material models and element designs to be implemented into FE programs. Among the numerous different elements that exist today, an important innovation in the FEM world was the implementation of interface elements. The need for elements became clear when the responses or a structure in the numerical simulation were not representative of what was happening in reality. Interface elements can be used in circumstances where there are two different materials adjacent to each other and are sliding. They can also be used for bridge elements with different number of nodes and degrees of freedom. However useful the interface elements are in the FEM for approaching realistic structural responses, their implementation can be troublesome. If interfaces are not implemented correctly in the FE model, they can lead to erroneous results and unstable numerical calculations. This can lead to designers avoiding the use of interface elements for simplicity. The implementation of interface elements and other innovations in the world of FE is powered by the constant need to bridge the gap between the physical domain and the numerical one. In the physical domain, in the case of structures, there are a multitude of variables that contribute to how the structure responds to the environment in which it exists. All of these variables are indirectly or directly related to each other and they all contribute in some way to the real structural response. When an attempt to model a real response in the numerical domain is made, in general there are assumptions an approximations made in an attempt to account for the unknown or immeasurable parameters. Hence, this becomes the main challenge in numerical methods and is the main focus of this dissertation.

A scaled masonry arch bridge was constructed and tested in 2001. This dissertation is about modeling the response produced by the experiment using 3D finite element analysis. Specifically the objectives for this dissertation are as follows:

1. Possess a solid understanding of the behavior of masonry arches under loading
2. Generate a suitable model using Finite element analysis and compare the results with the experiment

3. Design a simple method for incorporating interfaces into an FEM model

A previous study of the same experiment had already been completed. The goal was to continue the research of the numerical and decide which parameters of the bridge most closely simulated the experiment. However the data was not able to be validated and it became necessary to design a new FEM model.

This dissertation will begin by explaining the state of the art of masonry arch structural analysis and FEM modeling. Then the experiment to model will be explained in detail and the results from the experiment discussed. The verification process of the previous dissertation models will be presented. It will be shown how the models were compared and why it was necessary to generate new models. The following section will describe the basic principles of FEM modeling. In this section, all the relevant material which will be discussed in succeeding sections is presented. The next section will discuss the generation of the new FEM models and compare the results to both the previous model and the experimental results. Following this will be a discussion regarding correlations and discrepancies with the experimental results and previous FEM models. In the discussion section the method by which the interfaces were incorporated into the model will be discussed. Finally there will be a section written on recommendations for future study followed by the conclusion.

2. STATE OF THE ART

2.1 Introduction

In this chapter, the current state of knowledge of the structural behaviour of unreinforced masonry arch bridges will be described. This section will be broken into several sections to describe the state of the art in the following categories:

- Masonry Arch Stability Theories
- Numerical Analysis Principles using FEM
- Automatic Interface insertion techniques

2.2 Masonry Arch Stability Theories

2.2.1 Thrust lines

Thrust lines are constructed by first dividing an arch into multiple real or fictitious voussoirs then drawing the resultant vectors of each voussoir until the load reaches the ground. Figure 2-1(a) shows a detailed example of half of a simple arch being evaluated using the graphical approach. The thrust line is composed of the resultant at each voussoir (highlighted in blue in Figure 2-1(b)). An arch is considered stable if there exists a thrust line solution where the thrust line is maintained within the boundaries of the arch. A different thrust line is generated depending on the location, direction and magnitude of the external thrust force. A plastic hinge will be formed when the tangent of the thrust line intersects the boundaries of the arch. There could be infinite thrust line solutions.

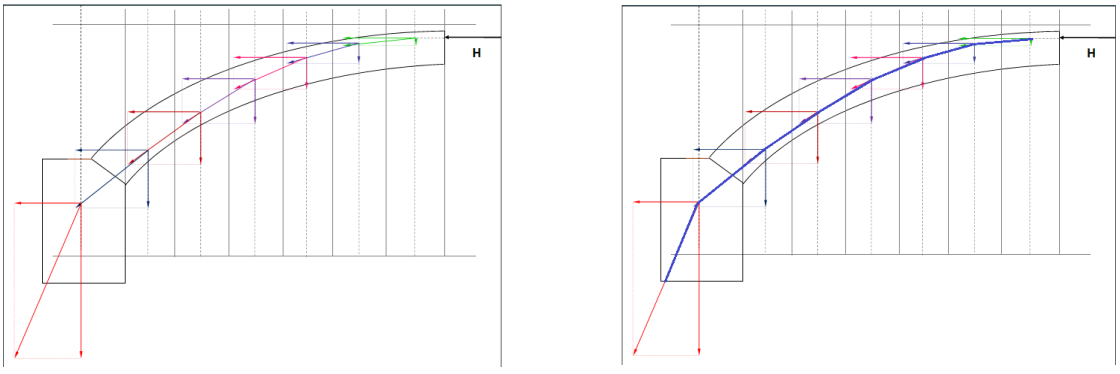

(a) (b) – Thrust line is highlighted

Figure 2-1:Example of the graphical method in use (Pere Roca 2011)

2.2.2 Limit Theorems

There are several methods of determining the stability and collapse mechanism of arches. Among them the most modern and accepted are the limit theorems of limit analysis, based on plasticity theory. If there exists and ultimate load or collapse load for an arch structure, then the lower-bound theorem determines a solution approaching from the safe side, and the upper-bound theorem approaches the ultimate load from the over loaded side as detailed in Figure 2-2 below:

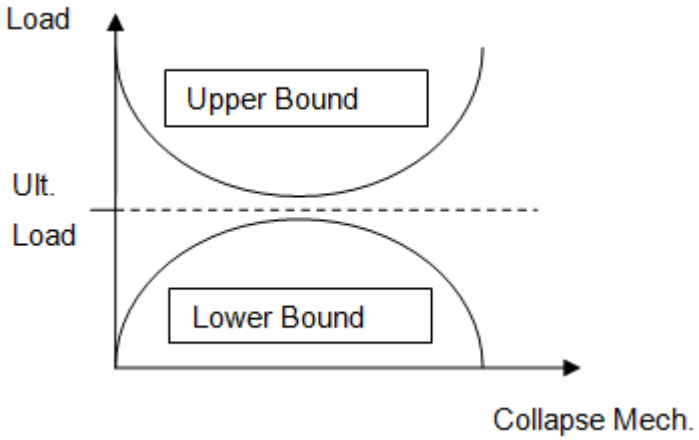

Figure 2-2: Diagram describing the limit theorems

Lower-bound (safe) Theorem:

As long as a thrust line solution can be found, the arch is considered stable.

Upper-bound Theorem:

If a kinematic mechanism can be found where the work developed by the external forces is greater or equal to zero, then the arch will fail.

Uniqueness Theorem:

If both a static and kinematic mechanism can be found, the load at which the mechanisms occur is the actual ultimate load of the arch structure.

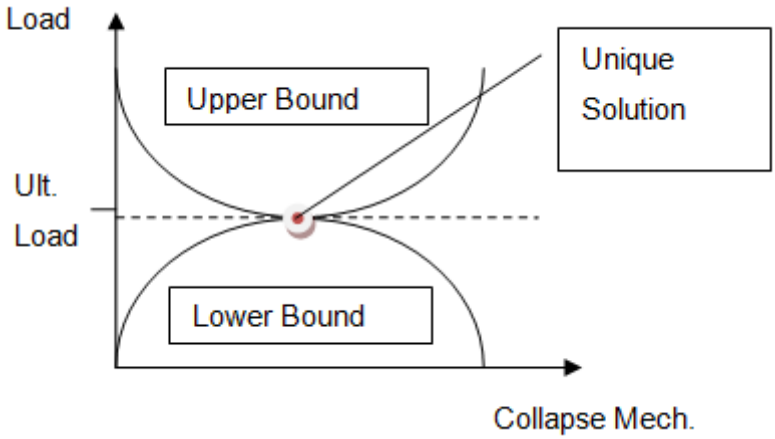

Figure 2-3: Demonstration of the uniqueness theorem

2.3 Numerical analysis Principles using FEM

2.3.1 Principle of the finite element method (FEM)

Consider a rigid body that is discretized into *n* elements with each element formed by *m* nodes. The rigid body is externally loaded by a traction **t** and its own weight, or body forces **b**. Vectors **t** and **b** are related to nodal displacements via the virtual work principle. The virtual work principle states that the virtual work done by internal forces within a rigid body is equal to the work done by the external forces acting on the same body. For each finite increment of $\mathbf{f}_{ext}$ or $\delta\mathbf{f}_{ext}$ the displacements of each node **u**(x) are related by a shape function matrix **N**(x) multiplied by a degree of freedom (dof) **d**. The **d** vector becomes the primary unknowns of the system of equations. The system of equations is formed by a displacement or rotation function for each dof. The boundary conditions are obtained by locations and types of supports. Once the system of equations is solved, the strains can then be calculated using the derivative of **N**(x), which is known as **B**(x) multiplied by **d**. Next, using the stiffness matrix **D**, the stresses at each node can be calculated from the strains.

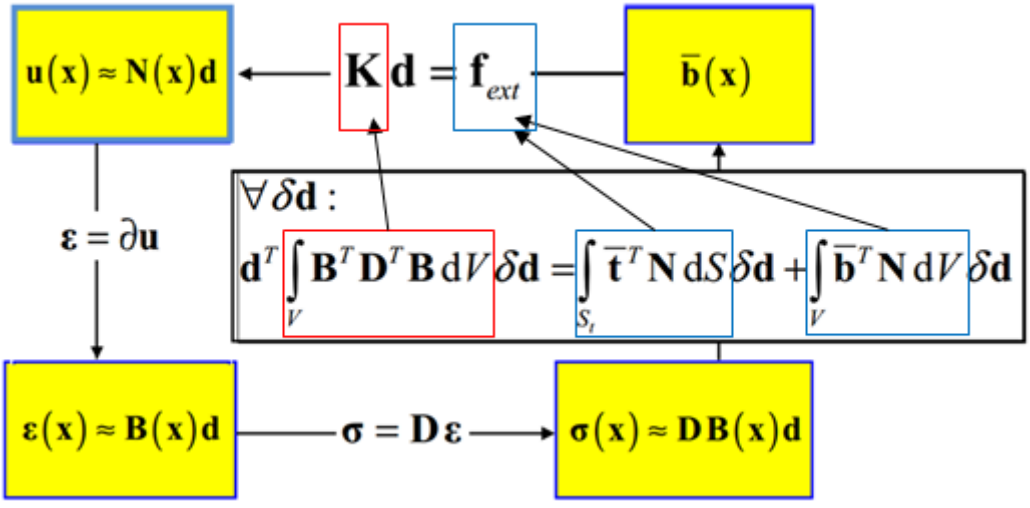

Figure 2-4: Summary of the FEM

2.4 Automatic Interface Generation

One of the objectives of this dissertation is to develop and innovative way of inserting interfaces into an existing model. This subject has already been explored by other researchers. An automatic mesh generation of interface elements was proposed by N.C Thai, T, Hasegawa, S. Aoyama and Z.L. Tun. In their proceeding “Automatic Mesh generation of Joint/Interface Elements This introduce a technique of automatically inserting interfaces between materials. Basically the program identifies different materials by the ratio of their relative stiffness and then it duplicates new nodes at the vertices of the material, relocates the material to the new set of duplicated notes and inserts an interface element in the newly created space. The figure below shows the method in action.

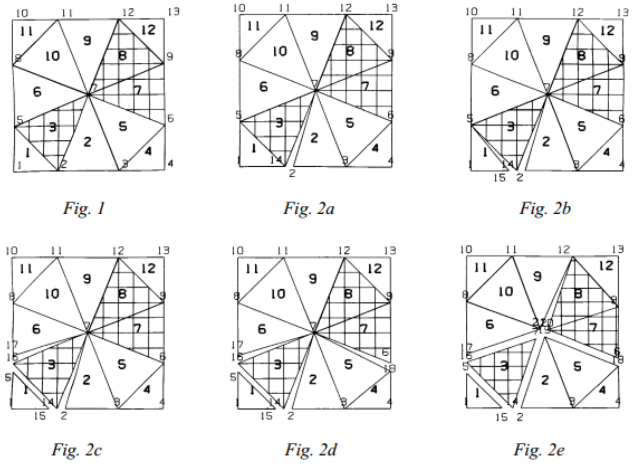

Figure 2-5: Example of automatic interface mesh generation (Thai, Hasegawa et al.)

3. EXPERIMENTAL TESTING PROCEDURE AND RESULTS

3.1 Introduction

Analyses were conducted on a segmental arch bridge. This section will describe the geometry of the structure and discuss the construction and testing procedures implemented. This bridge is part one of a two part experimental campaign on masonry arch bridges led by Professor Pere Roca and the department of Construction Engineering of UPC. This bridge was designed and constructed throughout the academic year of 2000-2001.

3.1.1 Bridge Geometry

The bridge geometry is described in Figure 3-1. Both the plan view and the elevation view can be observed in the figure below.

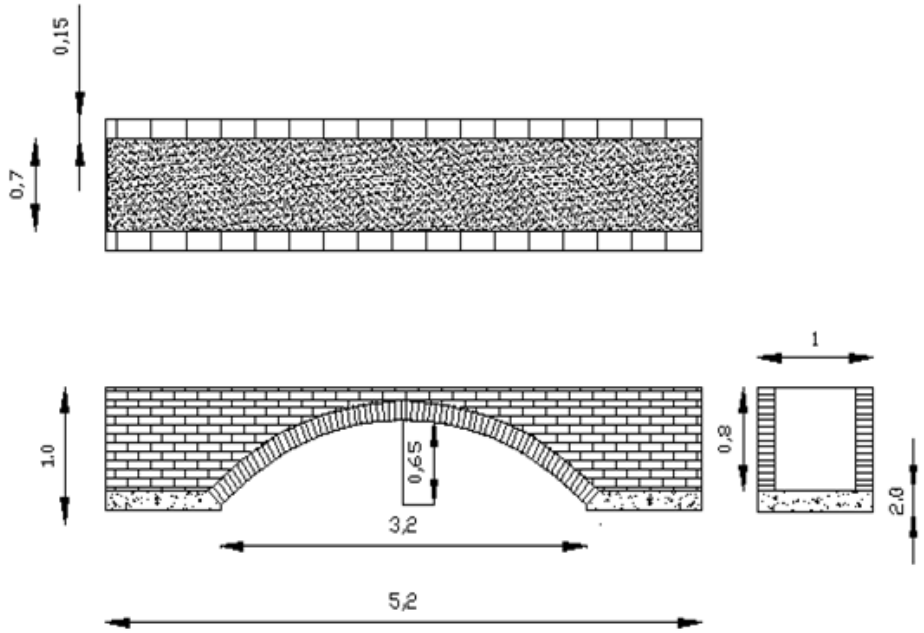

Figure 3-1: Segmental arch bridge geometry

3.1.2 Materials Used

Masonry

The masonry was constructed out of solid bricks with dimensions 13.5cm x 28.5cm x 4.5cm. This type of brick is known as 'totxo català' (Cai 2012). A total of 500 bricks were used to construct the structure. The masonry joints were filled with M-80 mortar and all the joints were filled flush. Test specimens were prepared for testing the compressive and shear strength of the masonry. The configuration of the

test specimens are shown in Figure 3-2. These specimens were tested in the UPC laboratory and yielded an average result of 19.6 MPa in compression and 0.363 MPa in shear capacity.

(a)

(b)

Figure 3-2:Masonry Configuration for Compression(a) and shear(b) testing

Abutments and infill

The abutments comprised of footings and the infill above. The footings were constructed out of reinforced concrete. The concrete slabs contained a total of approximately 400 L of concrete and the reinforcement was made of B500S steel rods. This resulted in an approximate weight of 40kg for the slabs. The infill consisted of loose sand, typically used in concrete mixtures. At various stages of filling, physical properties of the infill were measured. The results of these tests are outlined in Table 3-1.

Table 3-1: Physical soil properties for the segmental bridge

Physical Property	Value
Dry Density	1 550 kg/m3
Proctor Density	1 860 kg/m3
Friction angle	35-40°

The total weight of the structure is approximately 7 tones.

3.1.3 Bridge Construction Process

The bridge was constructed in the technical structural lab at UPC. First, the footings were constructed so there would be a solid foundation to build the structure upon.

(a) (b)

Figure 3-3: construction of footings (Serna 2001)

Next, the masonry segmental arch and spandrel walls were constructed using wooden centering.

Figure 3-4: Construction of ring and spandrel walls(Serna 2001)

Once the arch could support itself and the weight of the infill, the centering was removed and the steel profiles were constructed on each end. These profiles serve as a horizontal constraint on the arch as well as a container for the fill.

Figure 3-5: Method of assembly of the steel profiles(Serna 2001)

The steel profiles were constructed using the following steel sections:

- One steel sheet 100 cm x 100 cm x 5mm;
- Five 100 cm long vertical hollow square sections of dimensions 50x50x4 mm. These elements were welded to the steel plate;
- Four 118 cm long hollow rectangular sections 140x80x6 welded to the vertical sections. Holes were drilled at each end for the tie bars; and

- 8 steel bars of 25mm were threaded through the holes on the horizontal members and served as the ties.

Once the steel profiles were in place, the filling process could begin. The soil was filled and compacted.

Figure 3-6: Filling and compacting of the fill

A proctor test was completed for the infill in order to obtain density values for the infill. The dry density of the infill was determined to be 1560 kg/m3 and from the proctor test, the maximum density was found to be 1860 kg/m3 at an optimum moisture content of 6%. The results of the proctor test are shown below. It was determined that the friction angle of the infill was between 35 and 40°.

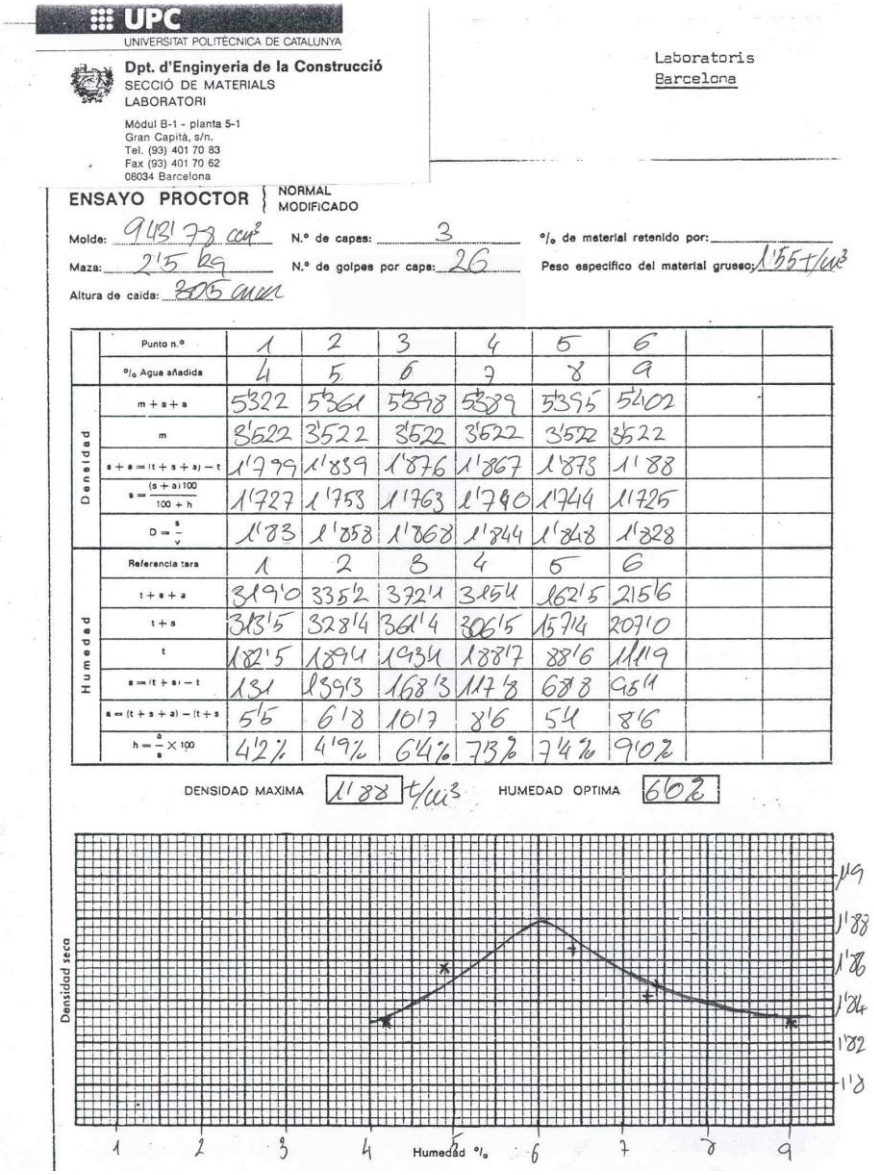

UPC
UNIVERSITAT POLITÈCNICA DE CATALUNYA

Dpt. d'Enginyeria de la Construcció
SECCIÓ DE MATERIALS
LABORATORI

Mòdul B-1 - planta 5-1
Gran Capità, s/n.
Tel. (93) 401 70 83
Fax (93) 401 70 62
08034 Barcelona

Laboratoris
Barcelona

ENSAYO PROCTOR { NORMAL / MODIFICADO

Molde: 9481'73 cm³ N.º de capas: 3 °/o de material retenido por:
Maza: 2'5 kg N.º de golpes por capa: 26 Peso específico del material grueso: 1'55 t/m³
Altura de caída: 305 mm

	Punto n.º	1	2	3	4	5	6
	°/o Agua añadida	4	5	6	7	8	9
Densidad	m + s + a	5'322	5'361	5'398	5'389	5'395	5'402
	m	3'522	3'522	3'522	3'522	3'522	3'522
	s + a = (t + s + a) − t	1'799	1'839	1'876	1'867	1'873	1'88
	s = (s + a)100 / 100 + h	1'727	1'753	1'763	1'740	1'744	1'725
	D = s/v	1'83	1'858	1'868	1'844	1'848	1'828
Humedad	Referencia tara	1	2	3	4	5	6
	t + s + a	319'0	335'2	372'1	315'4	162'5	215'6
	t + s	313'5	328'4	361'4	306'5	157'4	207'0
	t	182'5	189'4	193'4	188'7	88'6	111'9
	s = (t + s) − t	131	139'3	168'3	117'8	68'8	95'1
	s = (t + s + a) − (t + s	5'5	6'8	10'7	8'6	5'4	8'6
	h = a/s × 100	4'2%	4'9%	6'4%	7'3%	7'4%	9'0%

DENSIDAD MAXIMA 1'88 t/m³ HUMEDAD OPTIMA 6'0%

Figure 3-7: Infill proctor test results

In addition to completing a proctor test, densities were verified at various depths at the location where the load will be applied and above the point on the ring symmetrical to the load application. The density results are provided in

.

Table 3-2: Infill densities at various layers after compaction

Layer*	Under load	Symmetrical Location
1	1.92	1.93
2	1.98	1.96
3	2.01	1.98
4	1.94	2.05
5	1.89	1.90
6	1.93	1.98
7	2.02	1.99
* Layer 1 is the surface layer and layer 7 is the deepest layer		

The final step in the construction process was to install the testing apparatus and setup the data acquisition equipment. The final configuration of the experiment is shown in Figure 3-9.

(a) (b)

Figure 3-8: Picture of the loading cell and data acquisition equipment

The components in Figure 3-8 are written in Spanish. The translations are as follows:

Table 3-3: Translation of Spanish component names for loading equipment

Spanish Component	English Translation
Gato hidráulico	Hydraulic Jack
Célula de carga	Load Cell
Rótula cilíndrica	Rotary Cylinder
Perfil vertical para la transmisión de la carga	Vertical Profile to transmit load
Rótula esférica	Ball Joint for even load application
Perfil horizontal para el reparto de la carga	Hoizontal steel profile to disperse stress due to loading

The bridge is now constructed and ready for testing.

Figure 3-9: Segmental Bridge Ready for testing.

3.1.4 Instrumentation

Loading Cells

Loading cells were installed on the ties to measure the force on each bar. Only one side of ties are monitored with these load cells. There is also a load cell below the hydraulic jack to measure the applied load.

Embedded strain gauges

Four strain gauges were embedded in the infill directly underneath the point of load application at various depths:

Gauge 1: 28 cm;
Gauge 2: 46 cm;
Gauge 3: 58 cm; and
Gauge 4: 70 cm.s

Extensometers

Three extensometers are installed between the ground and the intrados of the ring. These extensometers are located along the symmetrical axis of the ring under the load, at the center of the ring and at a point symmetrical to the point of load application.

Figure 3-10: Placement of Extensometers

Data Acquisition Equipment

All of the above mentioned instruments were connected to a data acquisition device which acquires the data from all instruments and displays it on a computer.

3.1.5 Loading Process

The structure was loaded at a rate of 0.05 KPa/min. With a loading surface of 82 cm^2, this results in a load of approximately 10KN every 4 minutes. Throughout the loading process, the evolution of cracks was monitored and indicated on the structure. The evolution of the crack occurrences were documented as follows:

East and west side;
Cracks before 5 tonnes; and

Cracks between 5 and 10 tones.

Results are shown below in Figure 3-11.

Figure 3-11: Development of cracks during loading

The experiment went as expected until the load reached approximately 7 tonnes. Due to there being insufficient rotational constraints, the footings rotated outwards as shown in Figure 3-12.

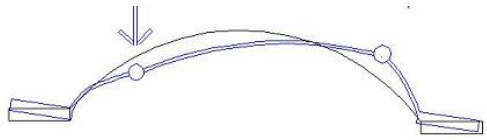

Figure 3-12: Rotation of footings during loading

When the footings rotated, it fundamentally created two hinges at the each end of the ring. This caused the collapse mechanism of the experiment to shift to the formation of two additional hinges rather than the expected 4 hinge collapse mechanism. This phenomenon is shown in Figure 3-13.

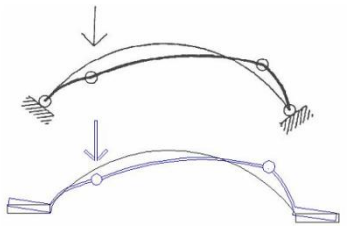

Figure 3-13: Diagram of the expected collapse mechanism (top) and the actual collapse mechanism after the rotation of the footings (bottom)

At 7.24 tones, two plastic hinges have been formed. One of which was under the point of loading and the other at the symmetrical location. In addition to the two hinges, there were cracks propagating through the infill and detachment material in the slabs and in the intrados of the ring. The collapse mechanism had clearly formed at this point and rupture was likely immanent. However, before the final rupture could occur, the structure was unloaded.

3.1.6 Analysis of results

The following data was collected by data acquisition equipment at 5 second intervals:

- Applied load from the load cell;
- Strains at the respective levels with respect to the embedded strain gauges;
- Deformation of the ring at the location of the three extensometers; and
- Load cells measuring the force in each tie bar on one side of the structure.

Applied Load Data

The load was applied at a rate of 1 tonne every 4 minutes. The rate was chosen to be slow enough to be able to sufficiently monitor the development of cracks throughout the loading process. The acquired data is shown in Figure 3-14. The ultimate load reached was 7.24 tonnes which is lower than expected. This can be explained by the rotation of the footings during loading.

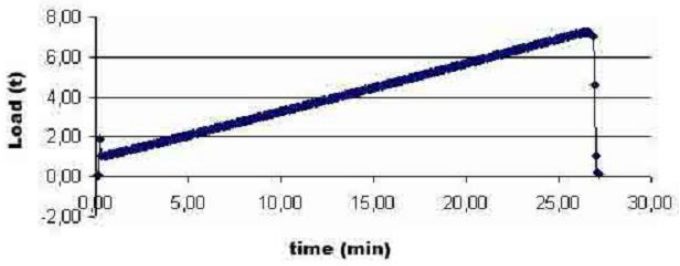

Figure 3-14: Applied Load over time

Embedded Strain gauges

The strain gauges were strategically placed to follow and verify the law of real passive resistance. The law states that the applied load increases until a certain point (one third of total depth) then recedes again due to frictional forces between the infill and the footing. This phenomenon is shown in the figure below.

Gauge 1: 28 cm (0.35 total depth);
Gauge 2: 46 cm (0.58 total depth);
Gauge 3: 58 cm (0.73 total depth); and
Gauge 4: 70 cm (0.88 total depth).

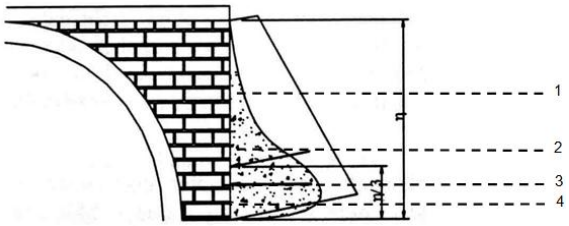

Figure 3-15: Law of passive resistance(Serna 2001)

From Figure 3-15 it can be seen that the third gauge is located approximately where the maximum stress is expected. The fourth gauge should show a decrease in stress due to the fictional forces between the infill and the soil. Unfortunately the third gauge yielded incorrect values so it was not possible to verify this phenomenon.

The gauges measure the strains in microns. These strains are related to the stresses by a gauge modulus (981 MPa). The results obtained from each gauge were as follows:

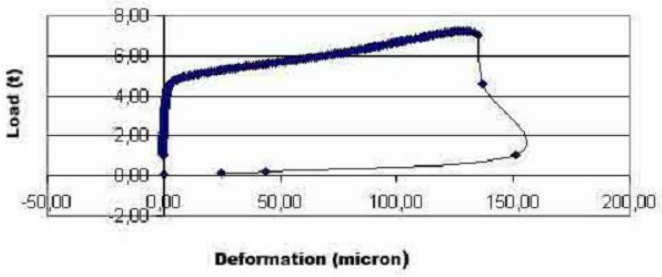

Figure 3-16: Strain gauge 1 data

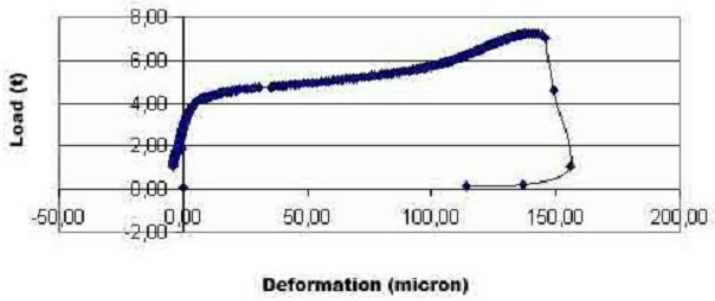

Figure 3-17: Strain gauge 2 data

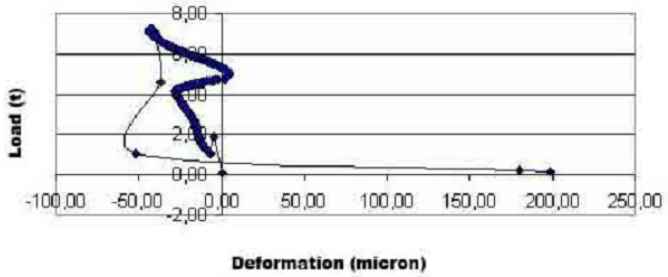

Figure 3-18: Strain gauge 3 data

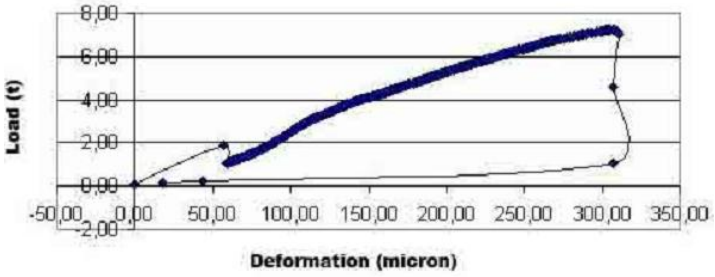

Figure 3-19: Strain gauge 4 data

The data from the third gauge was invalid and was most likely due to an equipment failure.

Both the first and second strain gauges experience very little displacement until the load reaches approximately 4 tones. This value coincides with the appearance of the first cracks (see Figure 3-11). It is reasonable to say that this is the development of the first hinge. Following the graphs of strain gauges one and two, they follow a similar slope until at approximately 6 tones, strain gauge two experiences a slightly larger rate of deformation while this is not evident in strain gauge one. Again upon inspection of Figure 3-11 the increase in strain gauge two coincides with the development of the second hinge.

The data obtained from the fourth strain gauge shows only a linear increase in deformations with no obvious changes of slope. It is well known that the young's modulus increases with the depth of infill. Therefore, it is likely that the stain gauge is deep enough to not feel the effects of the formation of each hinge due to the higher stiffness.

Extensometers

The following is the data obtained by each extensometer. (Serna 2001)

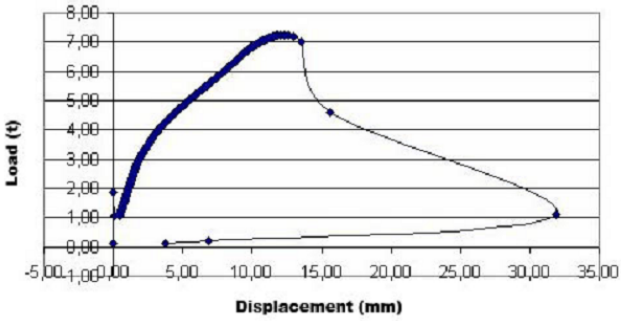

Figure 3-20: Extensometer (a) readings under the point of loading

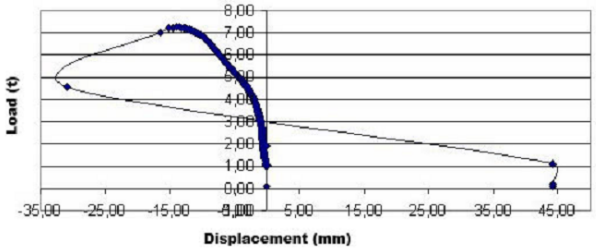

Figure 3-21: Extensometer (b) reading at the center

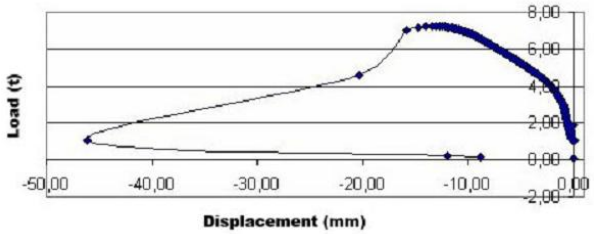

Figure 3-22: Extensometer readings (c) at the point symmetrical to the load

The key aspect to read from the three figures is the correlation of the change in and the appearance of cracks. Also, after each hinge is developed the slope of further displacements increases. This is an expected behavior once the structure starts to crack. The readings from extensometer a show the point as descending where as the readings from extensometer b show a rise. This correlates with the expected behavior of the arch. Finally from all three readings, it can be seen that the structure began to fail soon after the development of the second hinge.

It can be noted that there were no instruments set up to monitor horizontal displacements. However, these displacements would be far less in magnitude relative to the vertical displacements.

Tie Load cells

Figure 3-23 below shows the results obtained from each load cell attached to the ties. Gauge 1 refers to the highest steel tie and gauge 4 refers to the lowest.

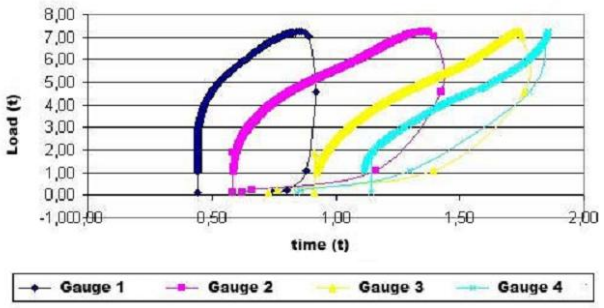

Figure 3-23: Readings from tie load cells(Serna 2001)

The initial values represent the initial load placed on the ties before implementing the test.

4. FINITE ELEMENT ANALYSIS OF THE BRIDGE

4.1 Introduction and Background

This section will discuss key principles involved in using software to conduct finite element analysis. Some of these principles are specific to the FE program where as others are general FEM analysis principles. This sub section will outline all the topics that will be discussed in section 1.

4.1.1 Geometry

When using the FE program, setting up the geometry is likely one of the most important steps when creating a model. This is because the way that the geometry is initially layed out will play a vital role in the success of the model and the time it takes to achieve results. Careful planning and future consideration are required before adding the first point or drawing the first line.

The first thing to consider is the dimensions of every geometric part. A geometric part is usually governed by differing materials or differing properties. In the case of analysing a generic masonry arch bridge, differing materials could be the infill and masonry ring parts where as differing properties could also be smaller element discretization in locations on the masonry ring where higher stresses are expected.

If interface elements are to be used, once all the required geometric parts are incorporated into the model, the future locations of interfaces should be considered. However, usually this is not an issue as the interfaces fall, for the most part, between different materials. However there are times where this is not so. For example in the case of masonry, an interface element could be modeled in the likely location of a crack.

4.1.2 Elements

There exists a multitude of elements available for use in FE programs. Only those used in the bridge model will be discussed. Each element has their own assumptions and methods of calculating the results. The type of element chosen depends on a number of factors such as:

- The geometry of the model
- The type of material being modeled
- The type of structural behaviour expected
- Precision of results required
- Numerical method used

Plane stress Elements (CQ16M and CT12M)

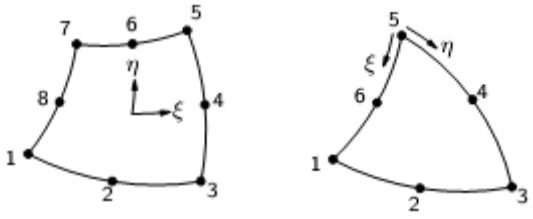

(a) (b)

Figure 4-1: Quadrilateral plane stress elements CQ16M (a) and Triangular CT12M (b) used in model(Diana 2009(Diana 2009)

Plane stress elements were chosen because the geometry of the bridge conformed to the principles of plane stress elements. They are:

- All of the elements lie in the same plane;
- All elements are loaded in the same plane; and
- The thickness is relatively small compared to the length and depth.

The general degrees of freedom of plane stress elements are translations in the x and y directions. The eight and six node plane stress elements were chosen rather than their four and three node counterparts. This results in higher order polynomial interpolations at each node. This will result in more precise stress readings. In FEM, the numerical solution for nodal displacements approaches the analytical solution at the nodes. However, with stress and strain, the numerical solution approaches the analytical solution at the integration points within the elements. Since both displacements and stresses are being evaluated in this dissertation, it was important to increase the number of nodes. The triangular elements were used when the geometry wasn't ideal for quadrilateral elements. The triangular element is actually an isoparmetric element with one end of the nodes collapsed into one. Therefore this element will yield constant strain, ε_{xx} over the element area where as the quadrilateral element will yield the following strains and stresses:

Exx/sxx: constant strain in the x direction and strain varying linearly in the y direction

Eyy/syy:. Constant strain in the y direction and strain varies linearly in the x direction.

Both elements yield constant shear strain over the element area.

Beam Elements (L6BEN)

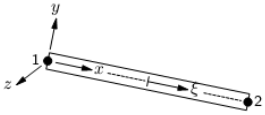

(Diana 2009)

Based on the *Bernoulli* theory, the general degrees of freedoms of these elements are x and y translations and z rotation. The steel profile can be approximated as a beam since the width is small relative to the depth. If plane stress elements were to be used here, there would be issues with element aspect ratios and the numerical calculation could become unstable. These elements have three degrees of freedom, x and y translations and z rotation therefore they cannot be placed next to plane stress elements without an interface as each element has different degrees of freedom. These class-I beam elements will yield a constant strain in the x direction. Deformations due to shear are neglected. The shear strain is partially accounted for by a shear strain correction factor and is constant over the cross-section.

Truss Elements (L2TRU)

(Diana 2009)

The steel ties were modeled using truss elements. The nodes of truss elements only have one degree of freedom, translation in x. Since the ties should not experience significant vertical deformations, these elements are most suitable. The element yields constant strain in the x direction.

Interface elements

L8IF

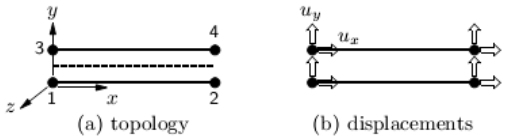

(Diana 2009)

CL12I

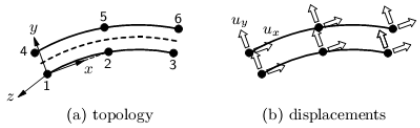

(Diana 2009)

These line interface elements yield the relative normal and tangential stresses between two elements. They are suitable for use between the plane stresses elements used in this model. The 3 node element was chosen to coincide with the eight node plane stress elements. This element is based on linear interpolation over the element.

Solid Elements (HX24L and TP18L)

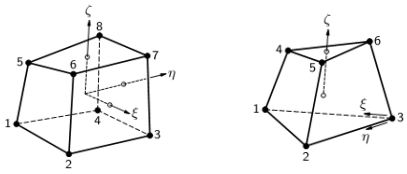

(Diana 2009)

The majority of the 3D model were modelled using solid elements. Each node of these elements has three degrees of freedom, x, y and z translations. The wedge elements and brick elements were used in locations where their geometry was well suited (triangular or square cross section). The less refined element was used to yield more stable numerical solutions and reduce the time required to carry out calculations. The wedge elements yield constant strains and stresses over the element volume. The brick elements yield the following strains and stresses:

exx/sxx: Strain/stress is constant in the x direction and varies linearly in the y and z directions.

eyy/syy: Strains and stresses are constant in the y direction and vary linearly in the x and z directions.

ezz/szz: Strains and stresses are constant in the z direction and vary linearly in the x and y directions.

Shell Elements (Q20SF)

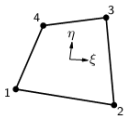

(Diana 2009)

Shell elements were used to model the steel profile. These elements are based on the theory of thin plates. The assumptions are as follows:

- The thickness is small relative to the other dimensions;
- All the nodes of the element lie in the same plane;
- All loads act in the plane of the elements; and
- Normal sections perpendicular to the surface remain strain after bending.

Plane interface elements (Q24IF and T18IF)

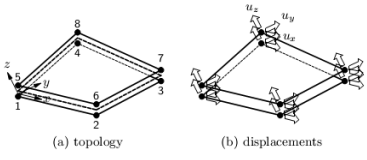

(Diana 2009)

These elements are used as interfaces between two planes. The general degree of freedom is relation translations normal and tangential to the element's surface.

4.1.3 Material Models

Material models serve to describe the constitutive equations which relate strain and stress after yielding (cracking, in the case of masonry). It will be important to have a solid understanding of the cracking model implemented for this dissertation. The material model used for nonlinear analysis of the Masonry is a smeared cracking model, total strain fixed cracking.

Multi-directional fixed crack model

This model uses strain decomposition in order to model the effects of cracking on the stress-strain relationship. Upon occurrence of the first crack, the total strain decomposes into an elastic strain and a crack strain as

$$\varepsilon = \varepsilon^{e} + \varepsilon^{cr}$$

The crack strain is a vector composed of normal and shear strains relative to the direction of the crack, in the *n-t* coordinate system as shown below.

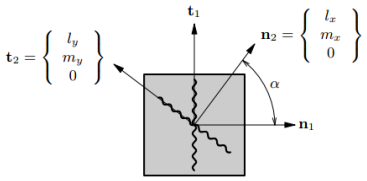

Figure 4-2: Crack normal and tangential vector components

In order for successive crack initiation to occur, two criterion must be satisfied simultaneously. These are:

- The principle tensile stress exceeds the maximum tensile stress.
- The angle between the principle tensile stress and the existing crack exceed the threshold angle.

There exists a crack strain vector for each crack existing in the element and by appending all of the strains into a vector, the assembled crack strain vector is formed.

The crack stresses are then considered to be a function of the crack strains with the following constitutive equation

$$\begin{Bmatrix} \sigma_{nn}^{cr} \\ \tau_{nt}^{cr} \end{Bmatrix} = \begin{bmatrix} D_{secant}^{\mathrm{I}} & 0 \\ 0 & D_{secant}^{\mathrm{II}} \end{bmatrix} \begin{Bmatrix} \varepsilon_{nn}^{cr} \\ \gamma_{nt}^{cr} \end{Bmatrix}$$

The secant stiffness parameters are specified as follows

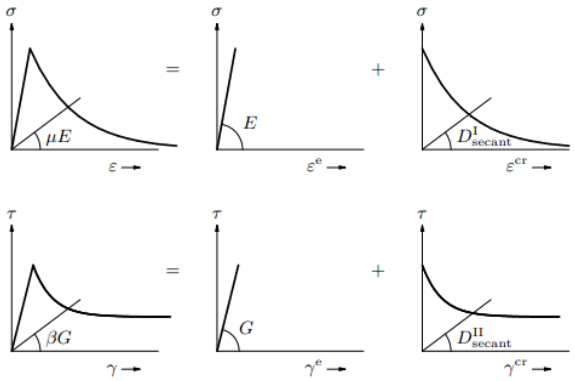

Figure 4-3: Illustration of stiffness softening parameters (Diana 2009)

Tension softening models

The rate at which the stiffness of the material reduces after cracking depends on the tension softening model. The model used for this analysis is linear softening.

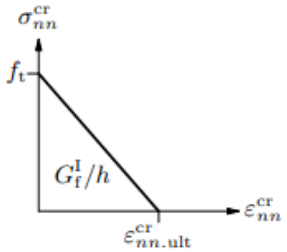

Figure 4-4: Linear tension softening model (Diana 2009)

Shear retention

Along with tensioning softening models, the FE program offers the analyst an option to reduce the shear modulus after cracking. There are two shear retention models available in the FE program and they are either full shear retention or constant shear retention. Full shear retention means that the material retains its full initial shear stiffness after cracking. Constant shear retention means that after cracking occurs the shear stiffness is reduced linearly until ultimate shear strain is reached, after which, the material feels no stress increase with increasing strain. For this analysis, constant shear retention was used.

4.1.4 Total fixed strain crack model

As an element is loaded, for each load increment, the FEM software calculates the strain increment for each element. In a rotating crack model, the principle strains, and therefore the crack strains are updated with each strain increment. In a fixed strain crack model, the crack strain is fixed upon the first crack initiation.

4.1.5 Interface Models

The stresses and strains are given in the *n-t* coordinate system as demonstrated in Figure 4-5. The models are based on a relation between the relative tractions and displacements in both the normal and tangential directions.

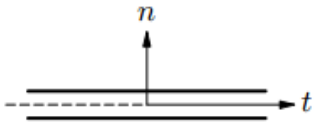

Figure 4-5: Coordinate system of interface elements

The linear constitutive relation is given by the following equation:

$$\begin{Bmatrix} t_n \\ t_t \end{Bmatrix} = \begin{bmatrix} \mathrm{K}_n & 0 \\ 0 & \mathrm{K}_t \end{bmatrix} \begin{Bmatrix} \Delta u_n \\ d_t \end{Bmatrix}$$

K_n and K_t are initial stiffness values assigned to the interface elements. In the nonlinear analyses, the interface elements follow a frictional model.

4.1.6 Meshing Refinement

The mesh of the model should be suitably discretized to yield accurate results as well as be able to efficiently carry out the numerical calculations. A mesh should be refined in areas where significant stresses or strains are expected. Conversely, areas where there is little or unvarying stress or strains, coarser meshes can be used for ease of calculation. A mesh can be refined in three ways:

h-refinement: Smaller division of geometry – Results in more elements per unit of surface area or volume

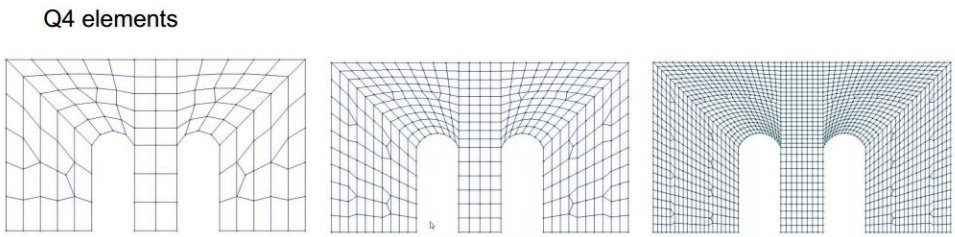

(Kabele 2011)

p-refinement: Higher order polynomial integration (more integration points) – adds additional integration points between existing nodes

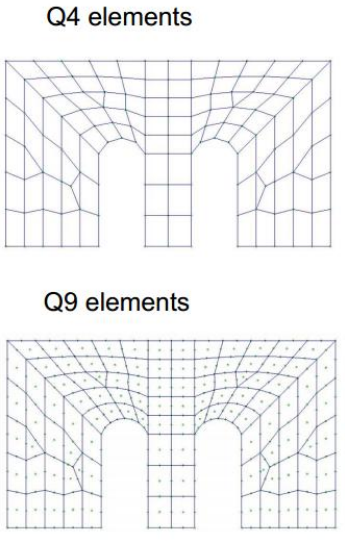

(Kabele 2011)

r-refinement: Moving Nodes – Meshing refinement technique to create fine meshing in areas of interest and coarse meshing in other areas. Once the nodes are positioned, then simply implementing a mesh division algorithm will automatically create a fine mesh in the areas of interest and a coarse mesh in other areas using the same amount of divisions.

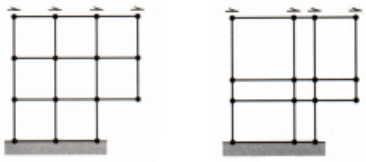

(Tech)

Stiffness matrix Singularity

This is an important concept in FEM as it is a common problem for numerical calculations. A singular matrix will result in a rigid body in the following circumstances:

Inadequate rigid body support to prevent rigid body motion

The geometry forms a mechanism

The rigid body contains elements of very low stiffness (damaged sections)

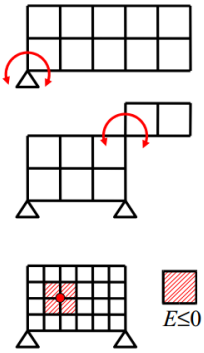

(Kabele 2012)

4.1.7 Method of Interface Insertion

Construct Gaps

This is the method which is written in the DIANA user manual. The steps that are suggested are as follows:

- Create the geometry of the structure and pre-allocate space for all the interfaces by including temporary “gaps” in the geometry.
- Attach any relevant properties to the interface elements and verify them while the gap is open.
- Once the properties and discretization of the interface elements have been verified, close the gap by moving one side on top of the other (in the case of a zero thickness joint).

The idea behind this method is that the user can visually verify that the interface elements are successfully generated, discretized properly, and possess the correct attributes before closing the gap.

However, depending on how the initial geometry was set up, this method can yield erroneous results. FE programs possess several algorithms for generating meshes. If the user is not willing to set up the mesh node by node, and element by element, they will generally take advantage of the FE program’s meshing algorithms. The algorithms are based on the user inputting their desired divisions of their existing geometry. For example, a user can choose a certain number of divisions for any line, surface or body in their model. Additionally, the user can specify exact element sizes, if it is more suitable..

When the FE program creates a mesh, it uses the existing orientations of the lines or surfaces in which they are created in as their own. If a surface exists between for nodes 1 2 3 and 4, the order of the nodes, by which the surface is defined, will define the orientation of the elements it contains. Whether creating geometric parts individually or having them created by the FE program, (in the case of importing models generated in AutoCAD) the parts are likely to not be uniformly oriented. Orientation of the elements local axes is not significant for most elements. For example, if you have a quadrilateral plane stress element (Q8MEM), when the element’s nodes experience displacements

then the FE program determines whether or not these displacements results in nodes becoming further apart (tension) or becoming closer together. Regardless of the orientation of the local axes, the nodes have fixed relative displacements. Conversely, the interface models calculate normal and tangential strains based on relative displacements. The relative displacements are not independent of the element's local axes.

In summary, the method of interface insertion explained by the FE program's user manual is useful in models with more simple geometry because the user can visually verify the properties of the interface. However, once the geometry becomes more complex, it becomes more difficult to keep track of where the joints are, which geometric parts must move to close the gaps, and which must remain still. Even before closing the gaps, the visual verification becomes more complex as well, especially in the case of three dimensional models.

Insertion into Data file

This is the method that was used to insert the joints into the segmental arch model for this dissertation. This method involves manipulating the data file generated by the FE program. The geometry of a model is created in the FE program's pre-processor called iDIANA. This program is a graphical user interface in which the model can be constructed. Once the geometry and meshing is complete, Diana outputs all the mesh data into a data file for use in analysing the structure. All relevant information regarding the mesh of the structure is written in the data file. This includes, but is not limited to:

- Model Info (title)
- Nodal coordinate;
- Element Connectivity;
- Element Materials;
- Element Geometries;
- Sets;
- Support Conditions;
- Loads; and
- Coordinate System(s).

The method is as follows:

1. Create the geometry of the model without interfaces. All future joint locations should coincide with the edge of geometric part and this must be reflected in the model. As you are creating the geometry, keep in mind the geometric parts (sets) that will be involved later for inserting joints. Ensure these sets are noted, specifically the nodes and elements included within them.

2. Generate a mesh and assign relevant properties and conditions such as:
    - Element Types
    - Materials
    - Physical Properties
    - Loads
    - Supports
    - Output the data file
3. Use a spreadsheet program (such as Microsoft Excel) to insert the joints
4. For the first joint to be inserted the following must be completed:
    - Create a new node set (duplicates of originals with new name)
    - Create new joint elements
    - Modify affected original elements to relocate them to the new node set
    - Update data file

    For subsequent joints the method is the similar.

4.1.8 Issues encountered with Interfaces

A critical item to consider is the orientation of the local axes of the interface elements. It is vital that the local axes of all the interface elements correlate with each other. This is because, contrary to regular elements, the stress vector depends on the direction of the local axis, as discussed in section 4.1.1. The interface elements do not calculate strains and stresses from virtual displacements on its nodes. Instead, they calculate relative stress (normal and tangential) from the surrounding material to which they are bonded between. Therefore, if the relative displacement between the two materials is in the direction of the positive local axes, the result will be positive. (In the case of stress, the interface will yield tensile results). However, if the interface were oriented opposite, the same relative displacements now yield a negative result (compressive stress). As long as the direction of the normal vector is kept consistent for all the elements, then it is easy to manipulate the data to show the correct results in the event they are disoriented. However, if the elements are oriented inconsistently throughout the model, then it will be difficult and tedious to manipulate every individual element in order to show realistic results.

For the 2D model, the interface elements should be subjected to a high concentration of forces at the location of the applied load. The forces on the other parts of the arch should be small in comparison as they represent the weight of the infill. As the depth of the infill increases, so too should the forces of the interface elements.

The figures below demonstrate the different orientations of the normal axis and the resulting normal forces between model B and model 2. The inconsistently oriented elements are evident in Figure 4-6 when comparing (a) and (b). The results of an inconsistent mesh are displayed in Figure 4-7 (a). At

the arches quarter span, the interface elements should be subjected to large normal forces due to the applied load. However in the inconsistent figures, at the arch's quarter span, some of the force vectors are pointing out from the extrados of the ring while the others are pointing inward. This results in high stress concentrations at the discontinuities and therefore leads to unrealistic and inaccurate results.

(a)

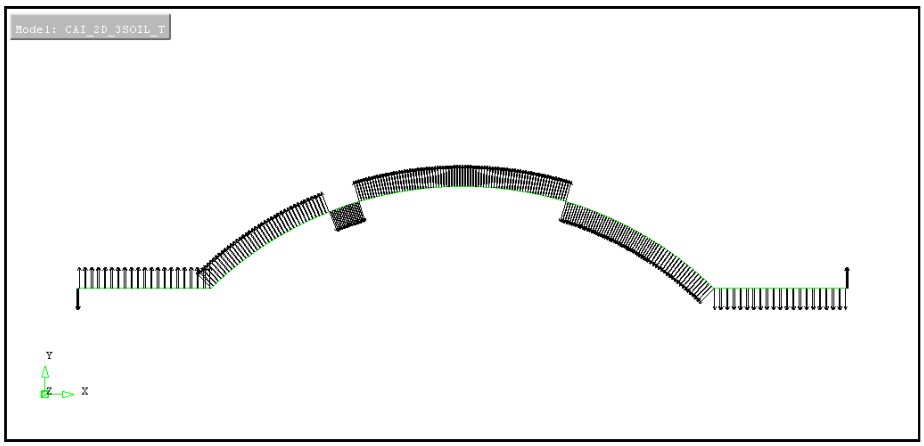

(b)

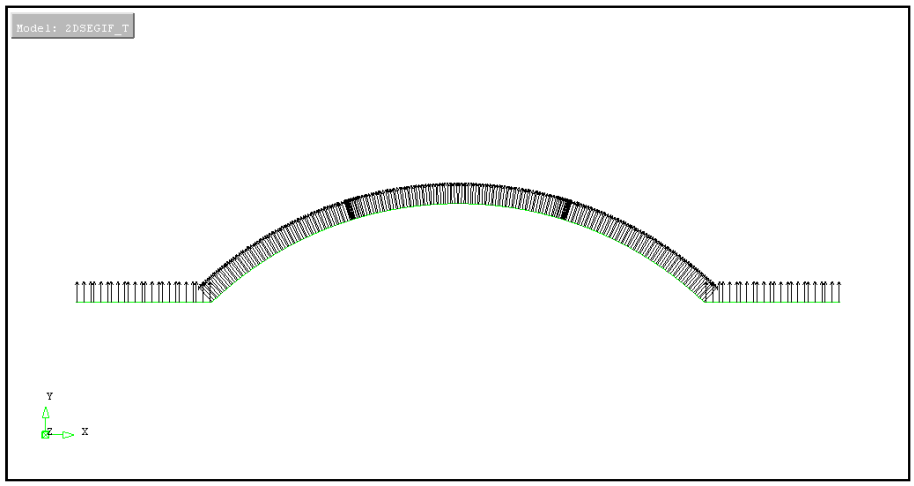

Figure 4-6: Demonstration of inconsistent (a) and a consitent (b) orientation

(a)

Max:0.13 MPa

Min:1.35E-5 MPa

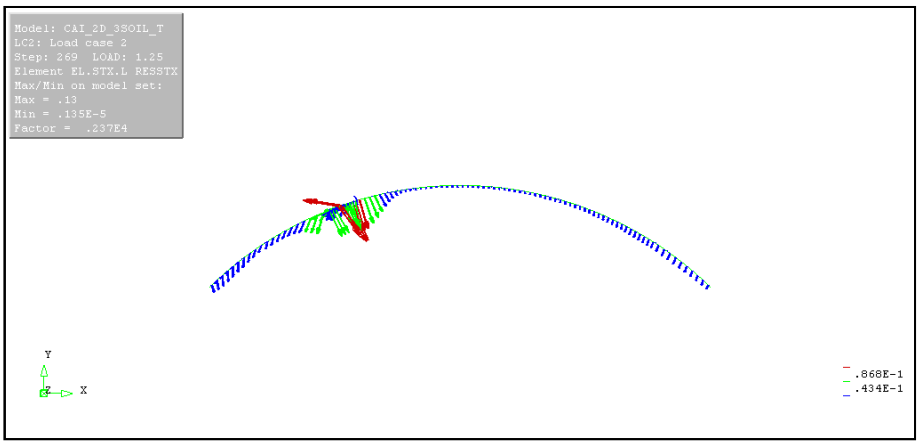

(b)

Max:0.0415 MPa

Min:1.95E-2 MPa

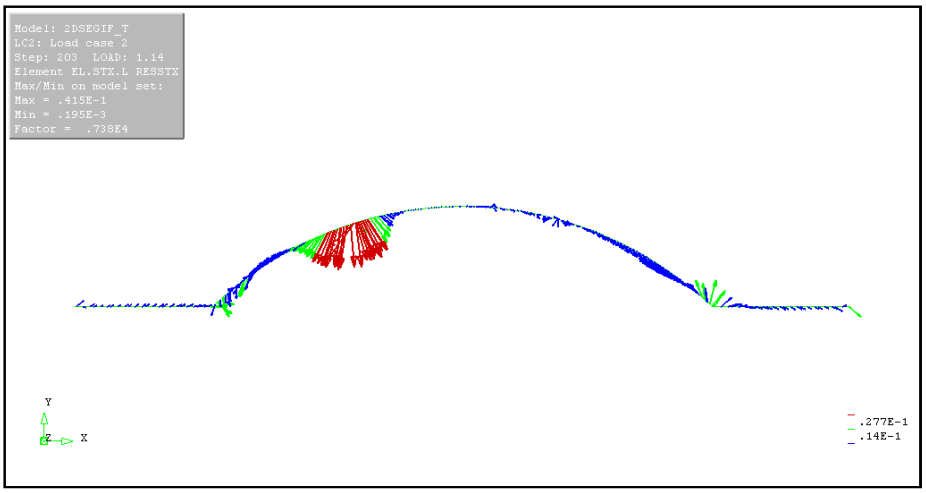

Figure 4-7: Interface element local force vectors Results due to orientation of IF elements

In The 3D model the lack of consistency in the orientation of the interface elements had been rectified for the most part. There were still some relatively disoriented elements located in the triangular mesh sections as shown below.

(a)

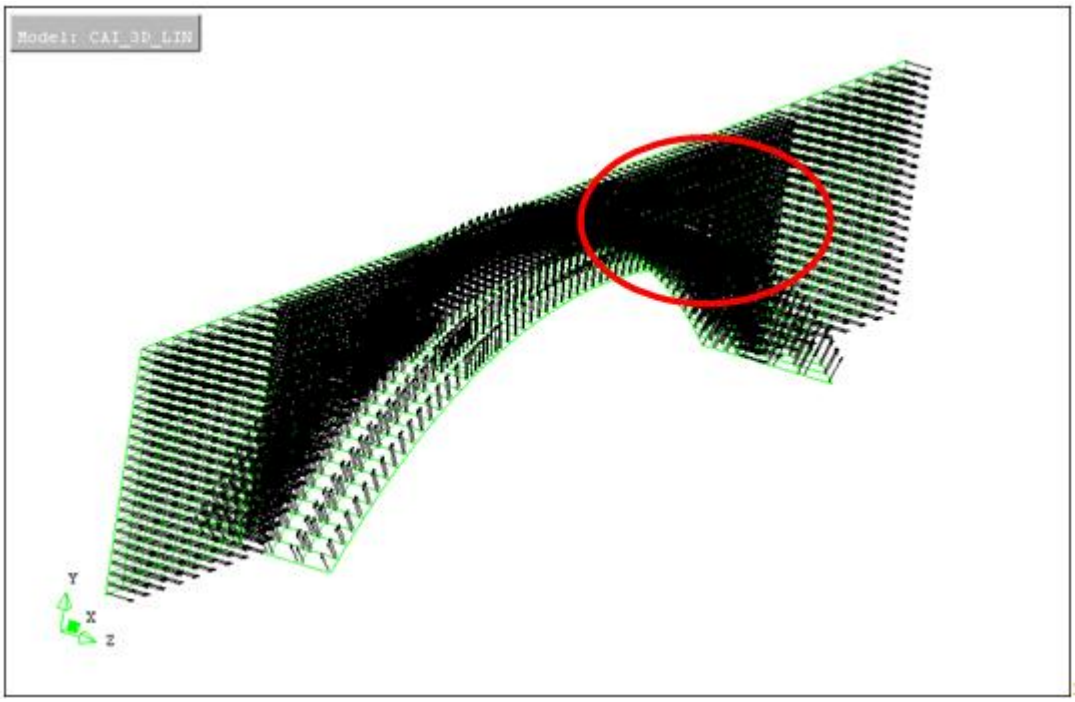

(b)

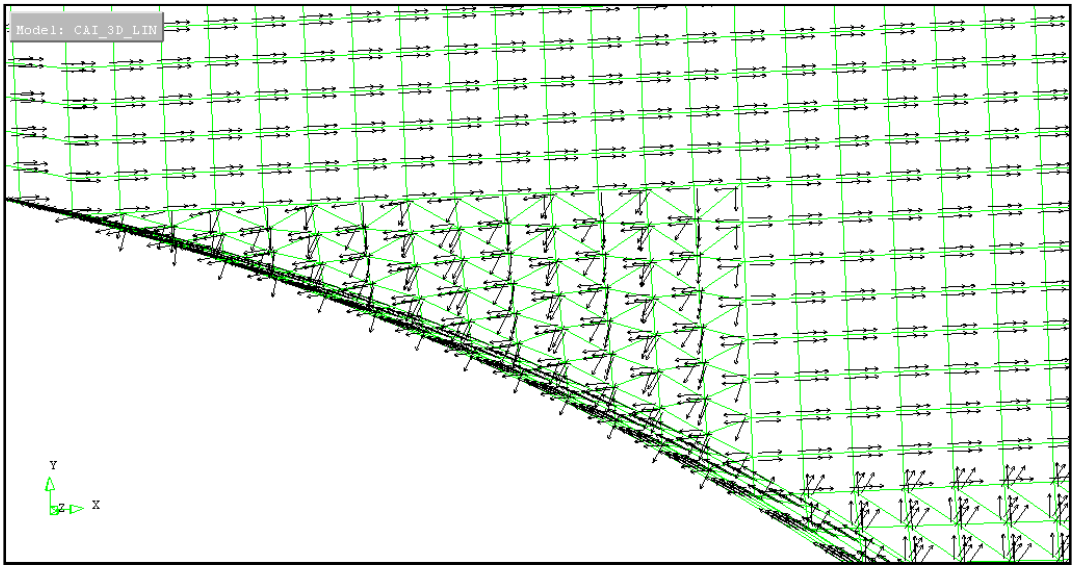

Figure 4-8: Interface normal axis orientation in model C (a) and the tangential axis (b)

One of the primary goals of the newly created models was to ensure all interface elements were orientated uniformly. This will produce more accurate and realistic structural responses.

5. PREVIOUS MODEL VERIFICATION

The research completed in the previous dissertation, was to be continued in this dissertation. It was necessary to verify the models. This verification was conducted by running a linear and nonlinear structural analysis using the same parameters and attempt to achieve the same or similar results. This not only ensures that the data contained within the previous files is in fact complete and correct, but also increases the confidence of results achieved from continued analysis on them. However, as will be discussed further on, not all of the models were able to be verified. After verification was unsuccessful, it became necessary to generate another model.

A summary of the bridge models that will be verified is written in the table below. The models will be referred to by these names for the remainder of the dissertation.

5-1: Summary of Bridge Models developed by Yunfan Cai

Model ID	Dimensions	Horizontal Constraint	Number of Soil Layers
A	2D	Supported	1
B	2D	Steel Bracing	3
C	3D	Steel Bracing	3

The construction of the 3D model had been broken down into simpler models. The first model constructed was a plane stress model. The next model had a steel tie and wall system for lateral constraint. This was to simulate the containment system in the experiment. Also, the soil was divided into three layers. Finally, the 3D model was generated. It consisted of half of the bridge in the experiment (lengthwise axis of symmetry).

5.1.1 Verification of Model A

The attributes used for verification of this model are discussed in this section. After the verification process, the model was able to be verified successfully.

Geometry

This model was the simplest model of the three. It was used for comparison with the analytical solution and as a stepping block for the 3D model. The structure was fully supported on the edges. The soil was modeled as one layer of soil with uniform properties. The objective of this model was to achieve the same collapse mechanism and shape of the deformed ring with the FE program.

Meshing

The mesh for model A is discretized evenly with a finer mesh generated for the ring elements and a coarser mesh used for the infill elements and footings. The ring is discretized with smaller elements to achieve more precise results in order to view the plastic hinges being formed. The average element size within the ring is approximately 50mm and in coarser locations the average element size increases to 110mm.

(a)

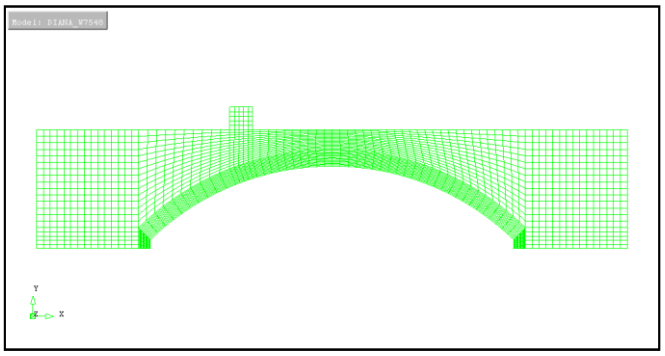

(b)

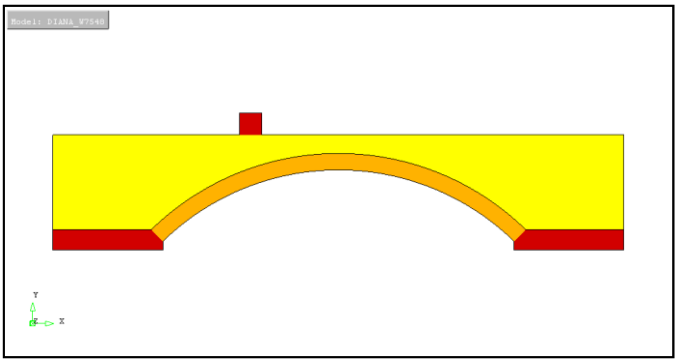

Figure 5-1: Mesh and materials (b) of model A

Material

For the most part, the materials for all the models were kept consistent to aid in model comparisons and result verifications. In some cases, the material properties of the soil were changed in future models.

5-2: Model A Linear Properties

	Soil (yellow)	Concrete(red)	Masonry (orange)
Young's Modulus [MPa]	37.78	34 000	5 120
Poisson's Ratio	0.2	0.15	0.18
Density [kg/m^3]	1 840	2 200	1 800

The masonry follows a total strain fixed crack model with constant shear reduction. (see section 4.1.4)

	Masonry nonlinear properties
Total Strain Fixed Crack Model	
Tensile Strength [MPa]	0.05
Mode-I Fracture energy	0.03
Compressive Strength [MPa]	21
Mode-I Fracture energy	5
Constant Shear Reduction Coefficient (β)	0.01

The interface elements followed the friction model between the surfaces of the masonry and concrete and the fill.

Table 5-3: Linear and nonlinear interface properties.

	Interface between infill and masonry	Interface between infill and concrete
Initial normal stiffness [MPa]	1.0E6	1.0E8
Initial tangential stiffness [MPa]	1.0E6	1.0E8
Density [kg/m^3]	1E-20	1E-20
Friction Model		
Cohesion	0.05	
Friction Angle	38	

Elements

The elements used in this model are as follows (see section 4.1.2)

Quadrilateral and triangle plane stress elements (CQ16M and CT12M)

- Infill
- Footings
- Ring

Line interface elements (L8IF) - Used in between infill and ring

Boundary Conditions

The model is fixed in the x and y directions along the base the footings and fixed in the x direction along the edges as lateral constraint.

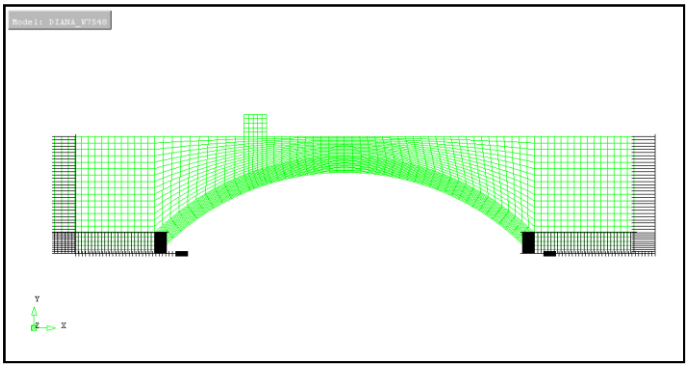

Figure 5-2: Boundary conditions for model A

Loading

The bridge is loaded by applying a pressure of 70 MPa over the area of the loading beam. Given the width of the beam is 200mm, this works out to a load of 14KN. The ultimate load on the experiment reached 7.24 tones. This is equivalent to approximately 70 KN.

Nonlinear results

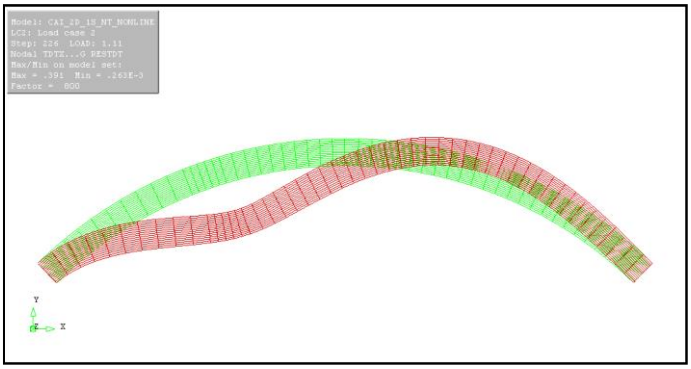

(a) Previous Dissertation	(b)
Max displacement: 0.395 mm	Max displacement: 0.391 mm

Figure 5-3: displacement results comparison

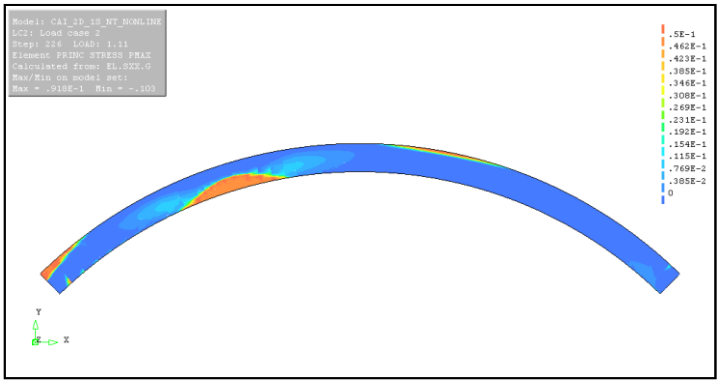

(a) Previous Dissertation	(b)
Max: 0.09, Min: -.104 MPa	Max: 0.0918, Min. -0.103 MPa

Figure 5-4: Stress results comparison

Verification conclusion for Model A

According to the images in the Yunfan's dissertation, the ultimate load achieved in the first analysis was approximately 15 KN. During the verification, a load of 18 KN was reached. Apart from this, when both models were compared at the same load level, the nonlinear analysis of each model yielded almost the exact same results, therefore this model can be considered verified.

5.1.2 Verification of Model B

In this section, the attributes used for verifying the model will be discussed. After the verification process this model was able to be verified.

Geometry

The geometry of model B is similar to that of model A. The soil has been refined into three layers with increasing stiffness as the depth of infill increases. This is to more closely model the behaviour of the fill. Also the model is no longer restrained on the edges. There is a steel profile and tie system in place to act as lateral constraints.

Meshing

The mesh is discretized similarily to model A as shown in Figure 5-5 (a).

(a)

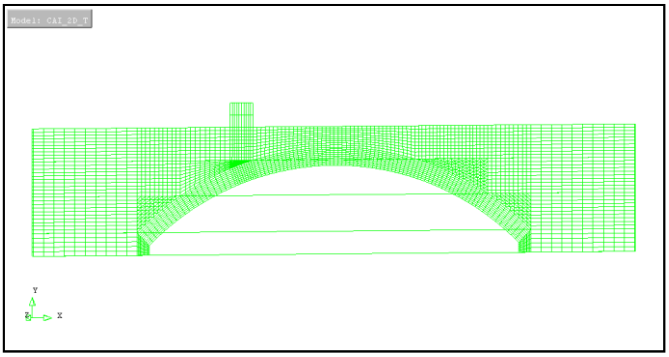

(b)

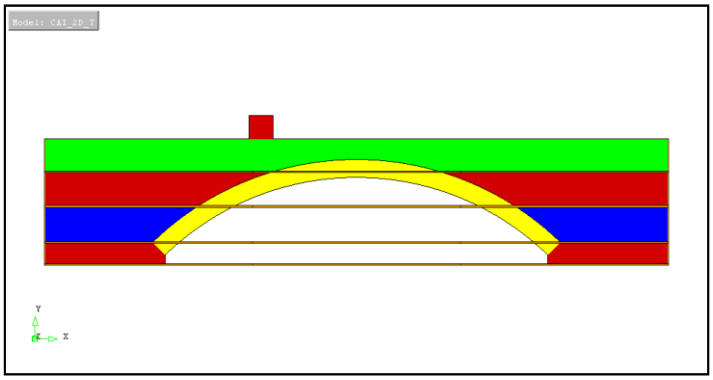

Figure 5-5: Meshing and Material Composition of model B

Materials

The material properties for the additional materials are outlined in the table below.

	Steel (Yellow-brown)
Young's Modulus [MPa]	200 000
Poisson's Ratio	0.27
Density kg/m^3	7 850

Table 5-4: Material properties for modified soil layers

	Soil A (Green)	Soil B (Red)	Soil C (Blue)
Depth [mm]	273	290	300
Young's Modulus [MPa]	4.352	13.38	22.82
Poisson's Ratio	0.2	0.2	0.2
Density [kg/m^3/	1 840	1 840	1 840
Friction Model			
Cohesion coefficient	0.02	0.02	0.02
Friction angle	38	38	38
Dilatancy angle	38	38	38

Elements

All of the elements used in model B are the same as model A except for the added steel elements. The steel profiles on the edges are simulated using plane stress elements (CQ16M) and the ties use truss elements (L2TRU). (see section 4.1.2)

Boundary Conditions

There are no longer horizontal supports because the structure is laterally confined with the steel profile and ties system. The mesh supports are shown in Figure 5-6.

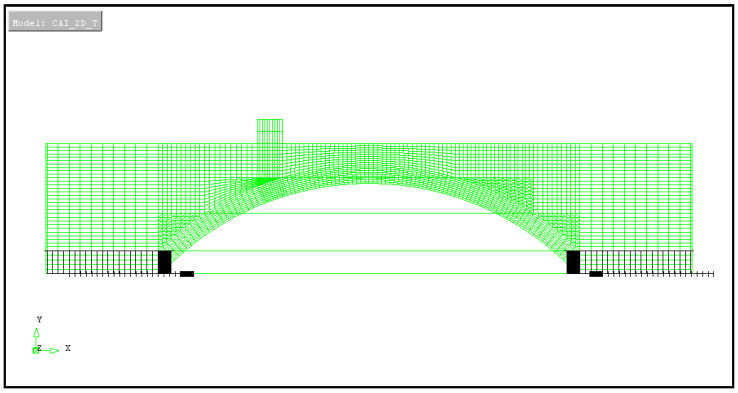

Figure 5-6: Boundary conditions for model B

Loading

The model is loaded the same as model A. 70 MPa of pressure are applied to the loading beam resulting in a load of 14KN.

Linear Result Comparison

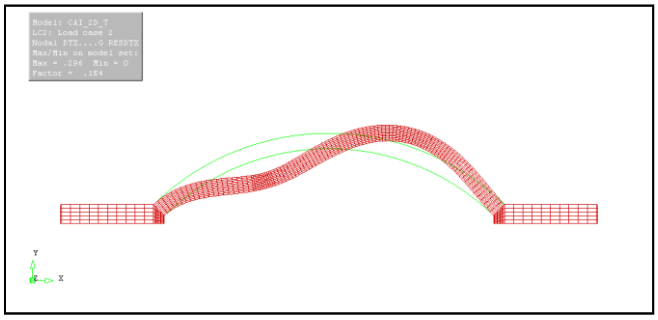

(a) Previous Dissertation	(b)
Max: 0.296 mm	Max: 0.296 mm

Figure 5-7: displacement results comparison

Both models yielded the same deformed ring mesh shape. The values are exactly equal.

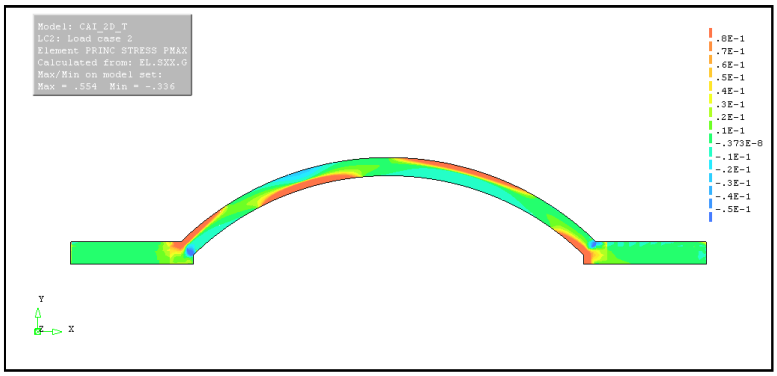

(a) Previous Dissertation	(b)
Max: 0.554, Min: -0.336 MPa	Max: 0.554, Min: -0.336 MPa

Figure 5-8: Stress results comparison

Both models yielded exactly the same responses.

Nonlinear results

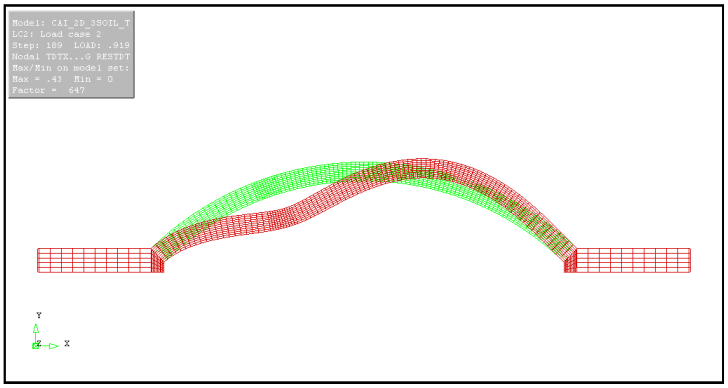

(a)	(b)
Max: 0.43 mm	Max: 0.43

Figure 5-9: Ring displacement results for both models

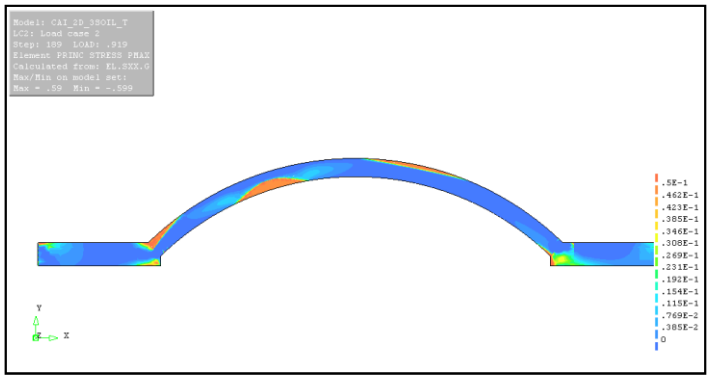

(a) Previous Dissertation	(b)
Max: 0.599, Min -0.599 MPa	Max: 0.599, Min -0.599 MPa

Figure 5-10: stress results for both models

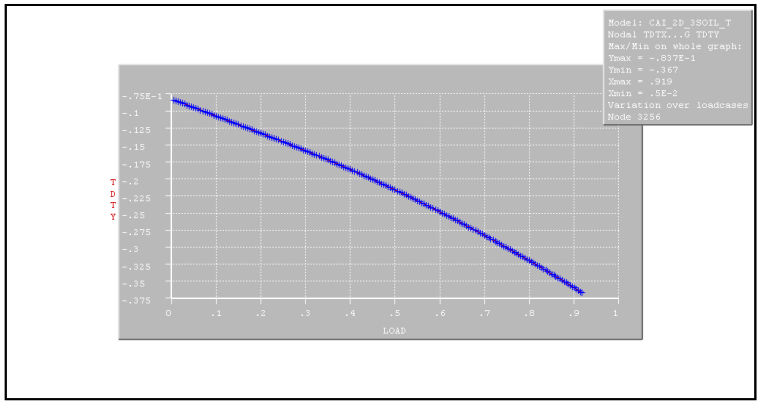

(a) Previous Dissertation	(b)
Max Displacement = -0.367 mm,	Max displacement -0.367 mm
Max Load= 12.9 KN	Max Load: 12.9 KN

Figure 5-11: nodal displacement under the point of loading for both models

Verification conclusions for Model B

The ultimate load achieved by the analysis for the previous dissertation was 12.9 KN. This is assuming that the load case presented in the dissertation was indeed the final loadstep. The ultimate load achieved during the verification process was 15 KN. This difference roughly the same order of magnitude larger achieved during the verification of model A. When both models were compared at the same load factor, they yielded the exact same results. Therefore, this model can be considered verified.

5.1.3 Verification of Model C

The attributes used to compare the linear results of model C are discussed in this section. The values were close in magnitude however the overall shape of the deformed mesh and the contour plots did not appear to match the results presented in Yunfan Cai's dissertation.

Geometry

The geometry of model C is basically that of Model B but swept out to three dimensions. For the sake of efficient numerical calculations, only half of the bridge was modelled. Due to the symmetry of the load and geometry along the length of the bridge, it was reasonable to assume half of the bridge should simulate the full structure. The loading beam was located over the fill and not on the spandrel wall as it is in the experiment. As well, the steel wall and ties are implemented as lateral constraints to simulate the same effect in the experiment.

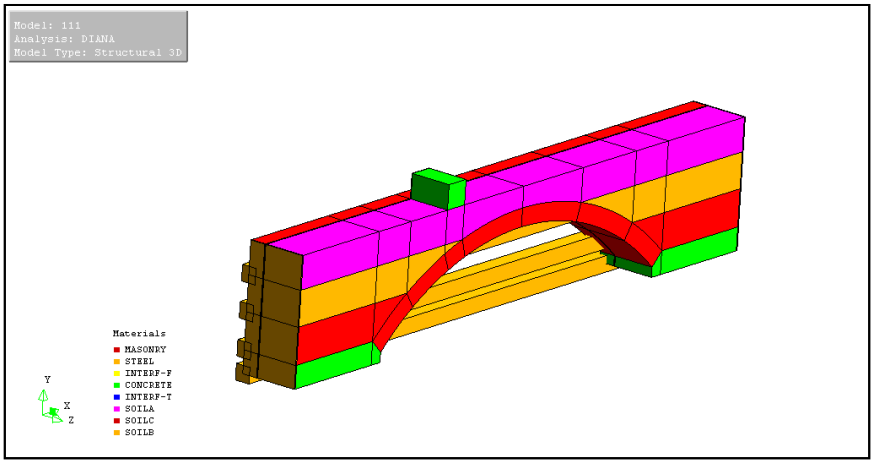

Figure 5-12: Geometry and materials of model C

Meshing

The meshing is similar to that of model B. It has been swept out to three dimensions and the only new division are the divisions along the thickness of the bridge. The elements within the spandrel wall had a length of 47mm where as those in the infill have lengths of 120 mm. The finer mesh in the wall will allow for more precise stress result at locations of interest, such as the interface between the infill and the spandrel wall.

Figure 5-13: Meshing of model C

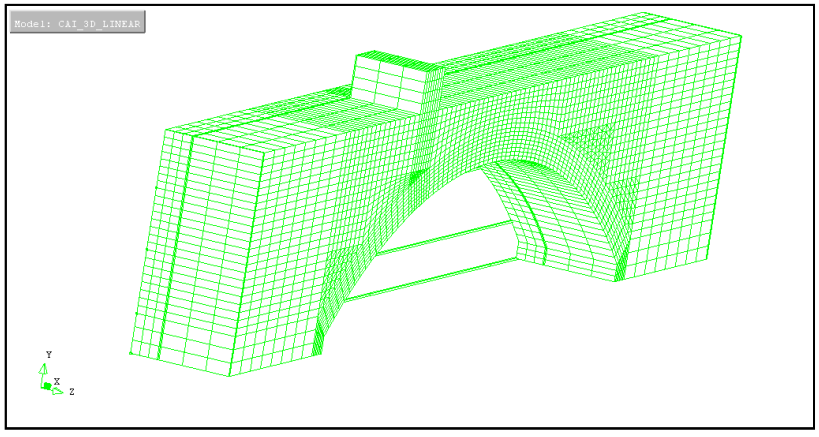

Materials

Most of the materials remain unchanged from model B to model C. The only difference exists in the material properties of the interfaces. The values for the initial stiffness of the interfaces were changed from 1000 GPa to 5 MPa. The change was made for the reason of reducing the tensile stress in the intrados of the ring. When stiff interface elements were used, the difference between the stiffness of the ring and interface was large, resulting in increased tensile stress on the elements in contact with

the interface. It was explained that though trial and error, when the interfaces had a stiffness of only 5 MPa, the residual stress in the intrados of the ring disappeared.

Elements

The elements used in the three dimensional model are outlined as follows (see section 4.1.2)

HX24L and TP18L brick and wedge elements – infill, masonry, footings, steel plate and loading beam

L2TRU truss elements – steel ties

Boundary conditions

The translations at the base of the footings are fixed for all three directions, x, y and z. Additionally, the axis of symmetry is restricted in translations in the z direction.

Loading

Bridge is loaded by a uniform pressure of 0.097 MPa. This pressure is applied to the top surface of the loading beam. This is equivalent to a load of 7 KN. Considering model C is only half of the actual bridge, this is a total load of 14 KN. The ultimate load during experimentation reached just over 70 KN.

Linear Results Comparison

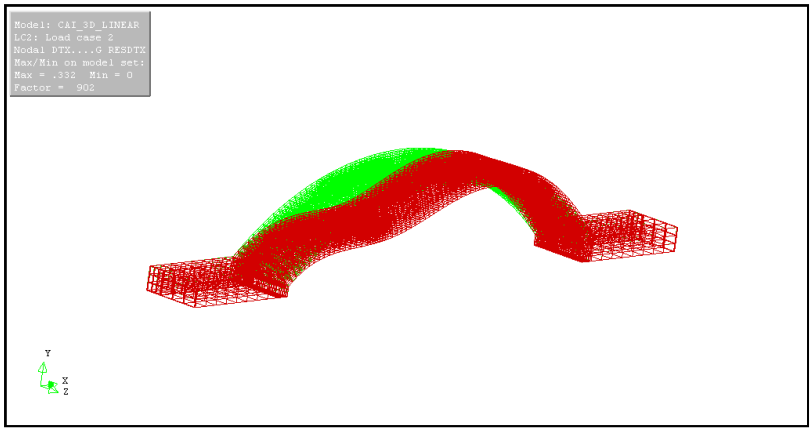

(a) Previous dissertation	(b)
Max = 0.332 mm	Max = 0.332 mm

Figure 5-14: displacement results for both models

(a) Previous dissertation	Max = 2.51 MPa Min = -0.514 MPa
(b)	Max = 2.51 MPa Min = -.411 MPa

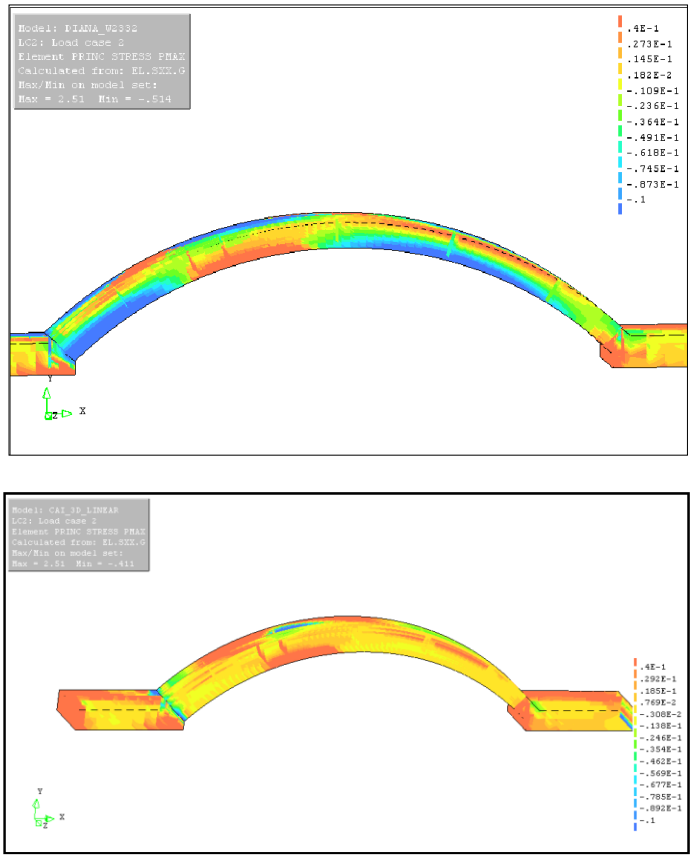

Figure 5-15: Differing stress results between models

Non Linear Result Comparison

A nonlinear analysis of model C proved to be unsuccessful. Using the data file from the previous dissertation and implementing the same analysis parameters written in the previous dissertation did not lead to a stable solution. The unstable quality of the model could possibly be originating from the in consistent orientation of the interface elements. However a more likely reason a converged solution could not be required can be seen in the linear analysis result.

Below, Figure 5-16 shows the outlined edges of the entire mesh of model C. In iDiana, when a discontinuity exists in the mesh it will be displayed with the VIEW OPTINONS EDGES OUTLINE option selected. Within this viewing environment, an outline will be displayed where ever one element is not connected to another adjacent element. Usually this occurs only at the edges of the model. However, in the figure there are several discontinuities present in the model. Figure 5-17 shows the same model only not including the interfaces in the view environment. New discontinuities exist but this is normal as there actually is no continuity between the ring and soil, or soil and wall element. The interface that was joining them is now removed creating a zero thickness gap. This figure helps to illustrate how IDiana displays gaps or discontinuities in the mesh. This is likely a result of the interface elements not being correctly attached with their surrounding elements. If these discontinuities exist, it

will lead to an ill-conditioned stiffness matrix. The condition of the matrix is defined by the ratio between the largest and smallest singular value. Without leading to a large discussion on numerical methods, basically the condition of the matrix is always greater or equal to one. When the condition approaches one, the matrix is considered well conditioned and the stiffness matrix can be inverted without many numerical errors. However as the condition of the matrix increases, it becomes more difficult to invert the stiffness matrix without the risking large numerical errors. When this happens, the matrix is considered ill-conditioned and when the condition number approaches infinity, the matrix is basically singular. In the case of a rigid body in FEM, the condition of the matrix increases with each discontinuity within the rigid body until the stiffness matrix becomes singular. Essentially each discontinuity circled in the figure is a finite location of zero stiffness within the rigid body. This is the most likely reason for not achieving a converged solution.

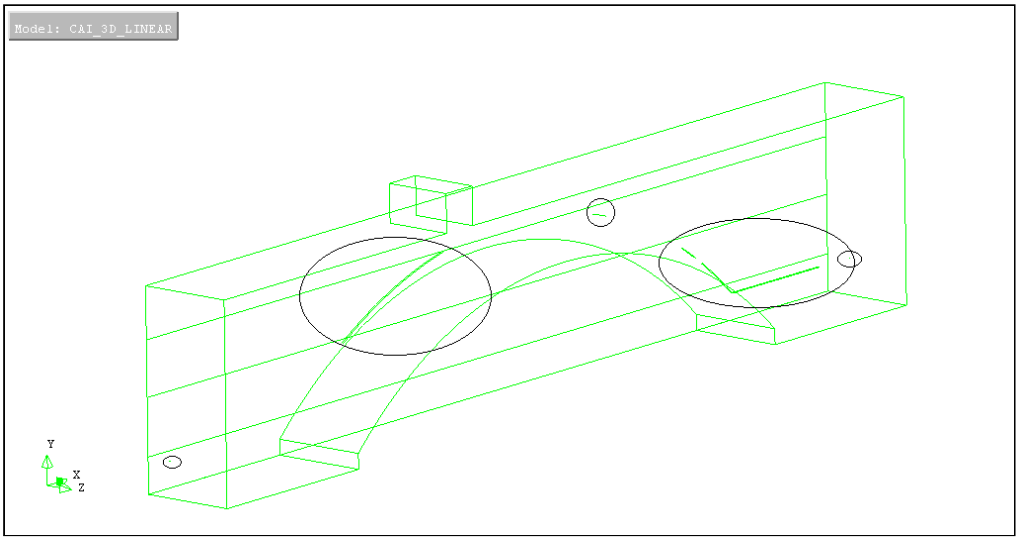

Figure 5-16: Model C with mesh discontinuities circled

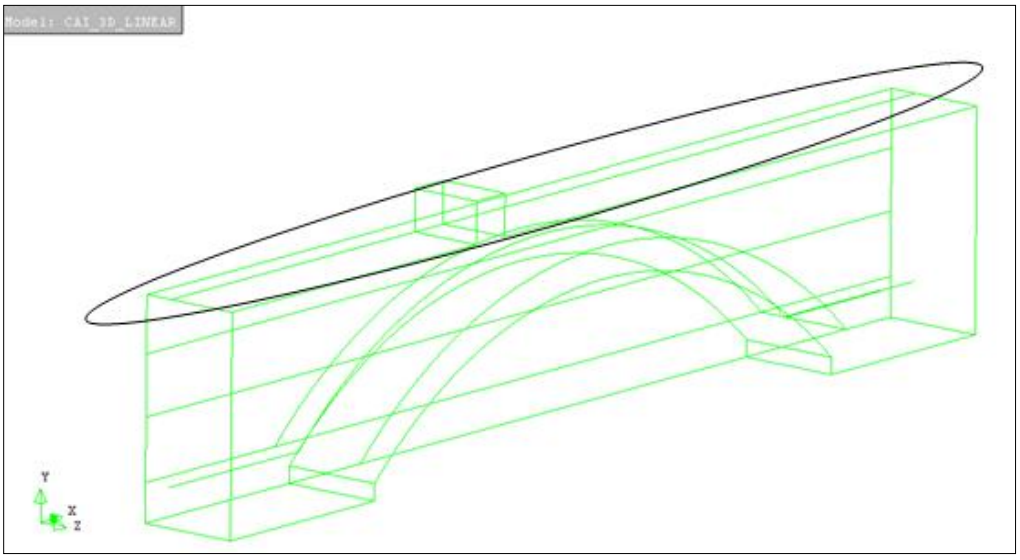

Figure 5-17: Model C mesh outline with interfaces removed (new gap circled)

Verification Conclusions for Model C

The comparison between the results presented in the previous dissertation and the verification models yielded similar results but not exact. Considering the same data file was used and a linear analysis was preformed, the values should be exactly the same. There does not seem to be a logical explanation to why there is less compression in the ring yet the tensile stresses are exactly the same. The same result occurs when the entire mesh is compared. The other anomaly is the fact that given the same model and inputting identical analysis parameters, no stable nonlinear analysis could be completed. One possibility is using a newer version of the FE program may yield different results, but this seems unlikely, especially in the case of linear analysis. Another possibility is the verified model may not have been the model presented in the dissertation. Perhaps it is an older version of the file used in the dissertation. Regardless of the reason, this model could not be verified. Therefore a new 3D model will be generated.

6. DEVELOPMENT OF NEW FE MODELS

The new model was developed considering both known issues with the previous models as well as recommendations suggested in the previous dissertation for further analysis. The recommendations for further study at the end of the previous dissertation were:

- Construct a finite element model with more soil layers
- Effect of different meshing discretization
- Effect of modifying the number of soil layers and changing the boundary conditions at the footings to reflect the rotations that took place in the experiment
- Analysis of the stresses in the steel ties

The geometry of the new model has five soil layers with their respective Young's modulus' increasing linearly with the depth.

Also, with models that utilize the steel ties, the ties now attach to beam elements (two dimensions) and shell elements (three dimensions). In the previous models, the truss elements connected to plane stress. In the new model, beam and shell elements were implemented using interface elements. Now the ties are attached to a rigid beam in the 2D model and a rigid plate. This setup should more closely resemble the support conditions in the experiment. With these conditions in place, the ring should be able to achieve larger deformations before collapse due to the added support of the beam and shell elements.

In the following sections the process of developing the new models will be described. Following this, results achieved including comparisons with the models from the previous dissertation and the experimental results will be presented followed by a discussion section.

Summary of models Developed

- The following table summarizes the created models. For ease of comparison, the geometry of each is similar to the previous models. The models will be referred to by the names listed in this table for the remainder of this dissertation.

Table 6-1: Summary of models

Model ID	Dimensions	Lateral Support	Number of Soil Layers
1	2D	Supported	1
2	2D	Steel Bracing	5
3	3D	Steel Bracing	5

6.1 Finite Element analysis of Model 1

Model 1 was created considering the existing geometry of model A. The method for inserting the interfaces for all the models was data insertion (see section 4.1.8)

6.1.1 Design Process

The design process for developing model 1 is outlined in the steps following this

1. The geometry was created using AutoCAD then imported into the FE Program.
2. Using the pre-processing interface, iDIANA, a suitable mesh was generated and discretized appropriately
3. Relevant properties were attached to the mesh such as materials, element types, physical properties, loads and boundary conditions)
4. The sets were created for use in implementing the data insertion technique of interfaces. The sets created were as follows:

Table 6-2: List of sets relevant to future IFR insertion

Set Name	Description
Ring	All Elements and nodes contained within the surface of the ring
Foot	All elements and nodes contained within the surface of the footings
IFR	All nodes contained on the line where the interface between the ring and fill is to be inserted

5. Export the geometry data to a data file.
6. Run a linear and nonlinear analysis on the model excluding interfaces to verify the created model so far.
7. Using a spreadsheet program such as Microsoft Excel, import the data into the spreadsheet to begin inserting the interface.
8. Identify the relevant sets created in step 4. The spreadsheet program should be able to filter the existing elements based on their whether or not their nodes or elements are contained in the sets.
9. For every node that is in set IFR, create a new node with identical coordintates. This will generate a list of the new nodes, referred to as IFR new nodes for this example. To assist in keeping track of the new nodes and old nodes, the new node list can be created in a known series such as 100s, 1000s, or 100000s. For example, nodes 11, 46 and 88 are in set IFR. Their new respective nodes will be 100011, 100046 and 100088. This arbitrary naming scheme is intended to remain the same when implementing interfaces into 3D models. The

series is made high enough so that it is unlikely that they will be surpassed by new nodes generated in more complex models. This will also make the insertion of the new IFR elements easier to keep track of.

10. Sort nodes in set IFR from smallest to largest x-coordinates.
11. Create new elements in between old nodes and new IFR nodes from one end of the bridge to the other. An example of the beginning of the spreadsheet be set up look like this:

x-coord	**0**	**115.906**	**231.8121**	**347.5621**	**463.3121**	**579.0621**	**…**			**5200**
Node	11	100	88	111	94	1632	…	2057	2069	46
Element	100001		100002	…	…	…	…	100100		
Type	CL24I		CL24I	…	…	…	…	CL34I		
n1	100011		100088	…	…	…	…	102057		
n2	100100		100111	…	…	…	…	102069		
n3	100088		100094	…	…	…	…	100046		
n4	11		88	…	…	…	…	2057		
n5	100		111	…	…	…	…	2069		
n6	88		94	…	…	…	…	46		

12. Once the new IFR elements are created, it is necessary to relocate one of the adjacent materials onto the nodes of the new set. In this example, the ring and fill elements were moved to the new nodes.
13. Every node in set FOOT and RING that coincides with the nodes in set IFR, must be modified to their new node in the 100000s series.
14. The interface is inserted into the model. The last step is to update the data file keeping in mind that the following sections may need special attention:
    a. Element geometry assignments for IFR elements
    b. Element Material assignments for IFR elements
    c. Sets can be updated to include new IFR elements
15. The data file is ready for analysis. The FE program DIANA, includes a program called Meshedit. It enables the user to visually represent the contents of the data file. It is especially useful to check the new geometry of the model, and the element property assignments.
16. Run analysis of new model to verify the correct structural responses of the interface elements.

Geometry

The geometry of this model was created similar to model A for the sake of comparison.

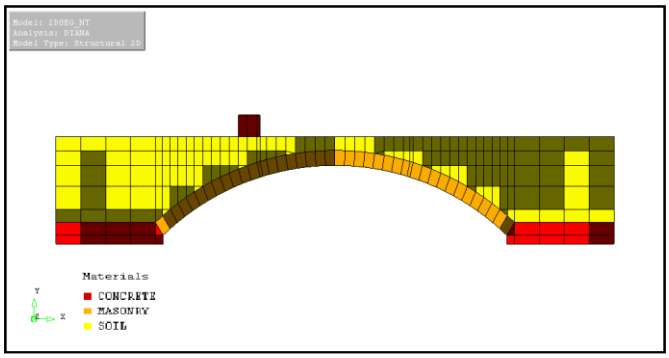

Figure 6-1: Geometry and materials of model 1

Materials

The materials used in this modal are summarized in the following tables.

6-3: Model 1 linear properties

	Soil	Concrete	Masonry
Young's Modulus [MPa]	37.78	34 000	5 120
Poisson's Ratio	0.2	0.15	0.18
Density [kg/m^3]	1 840	2 200	1 800

The masonry follows a total strain fixed crack model with constant shear reduction (see section 4.1.4). The properties of the model are written below.

Table 6-4: Model 1 nonlinear properties

	Masonry Properties
Total Strain Fixed Crack Model	
Tensile Strength [MPa]	0.05
Mode-I Fracture energy	0.03
Compressive Strength [MPa]	21
Mode-I Fracture energy	5
Constant Shear Reduction Coefficient (β)	0.01

The interface elements followed the frictional model between the surfaces of the masonry and concrete and the fill.

Table 6-5: Linear and nonlinear interface properties.

	Interface between infill and masonry
Initial normal stiffness [MPa]	1.0E6
Initial tangential stiffness [MPa]	1.0E6
Density [kg/m^3]	1E-20
Friction Model	
Cohesion	0.05
Friction Angle	38

Elements

The elements used are the same as those for model A, however the interface elements were modified to CLI9IF elements so that the integration points coincided and therefore achieve smoother results.

The elements used were in model 1 were (see section 4.1.2)

Table 6-6: Elements used in model 1

Material	Element
Concrete	Plane Stress (CQ16M & CT12M)
All infill	Plane Stress (CQ16M & CT12M)
Masonry	Plane Stress (CQ16M & CT12M)
Interfaces	CL9IF

Loading

A pressure of 70 MPa is applied to the top surface of the loading beam. This results in 14KN of load.

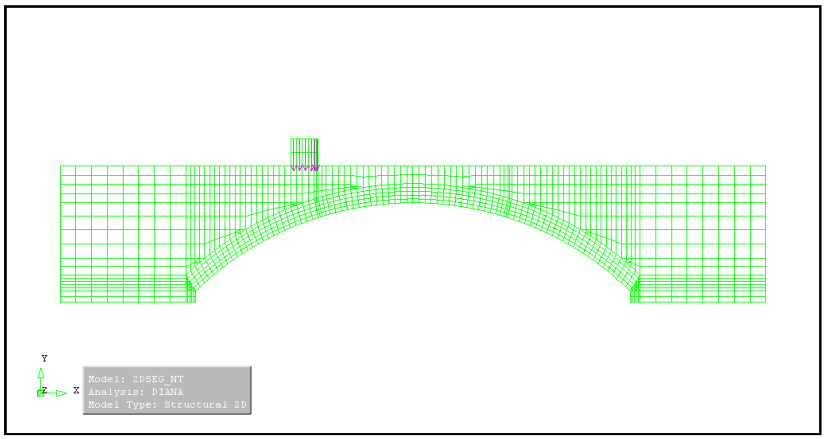

Figure 6-2: Model 1 loading conditions

Boundary Conditions

Model 1 has the same boundary conditions as model A.

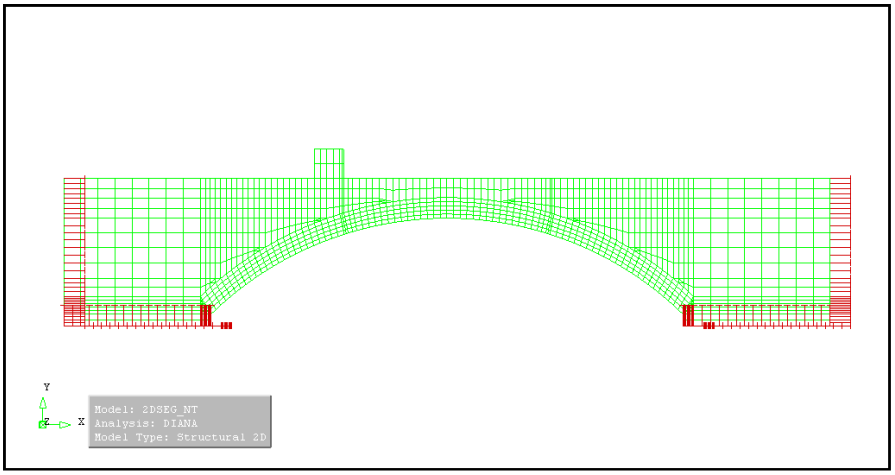

Figure 6-3: Model 1 boundary conditions

Model 1 Non Linear Results

Displacement Comparison

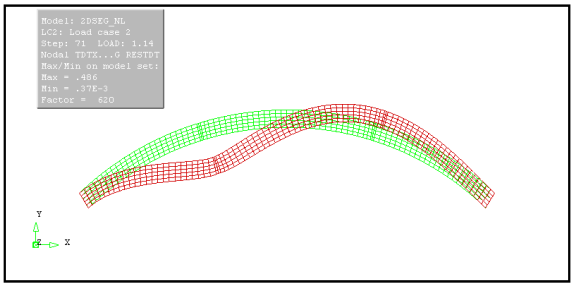

(a) Model A

Max: 0.395 mm

(b) Model 1

Max: 0.468

Figure 6-4: Displacement comparison for both models

Stress Comparison

Max: 0.0919 Min = -0.104 MPa	(a) Model A
Max: 0.145 *Min = -0.102* MPa	(b) Model 1

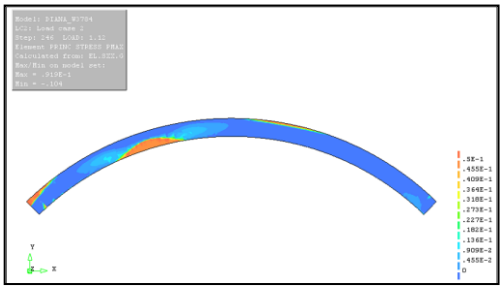

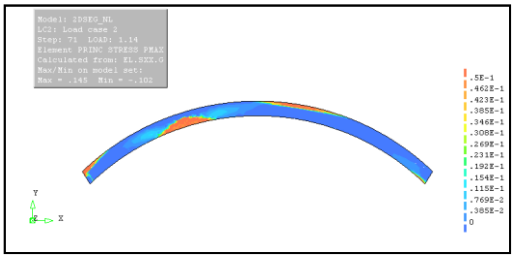

Figure 6-5: Comparison of stresses

Discussion of results

The results of these models do not seem to correlate well. The maximum displacement in model 1 was 0.468 mm where as in model A only reached 0.395 mm. When stresses were compared, Model A had a maximum principle stress of 0.145 MPa and a minimum of -0.104. Model 1 had a maximum principle stress of 0.145 MPa in the ring and a minimum of -0.104. Finally, it is important to note that the ultimate load reached by model A was 15.68 KN and for model 1, 18.34 KN. These discrepancies may be accounted for by the interface elements functioning incorrectly. Let us explore the interface details of each model and see how they account for the discrepancies.

The figures below show the orientation of the local axes in the interface elements.

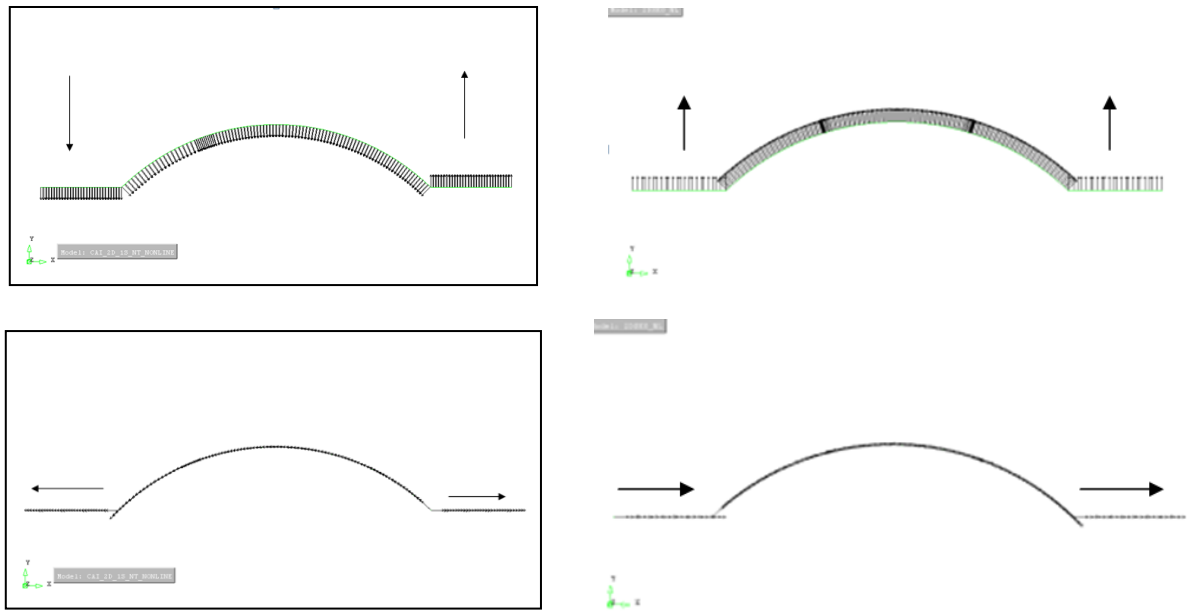

(a) Model A (b) Model 1

Figure 6-6: Comparison of Interface element orientation

It can be seen that the orientation of the axes is inconsistent in model A. The results presented in Figure 6-7 aid in demonstrating the importance of properly oriented elements. For this model, the only normal tractions that exist in the interface elements are due to the external loading and to the weight of the fill. As the weight of the infill decreases over the midpoint of the arch, the force should decreases proportionally as it does in Figure 6-7 (b).

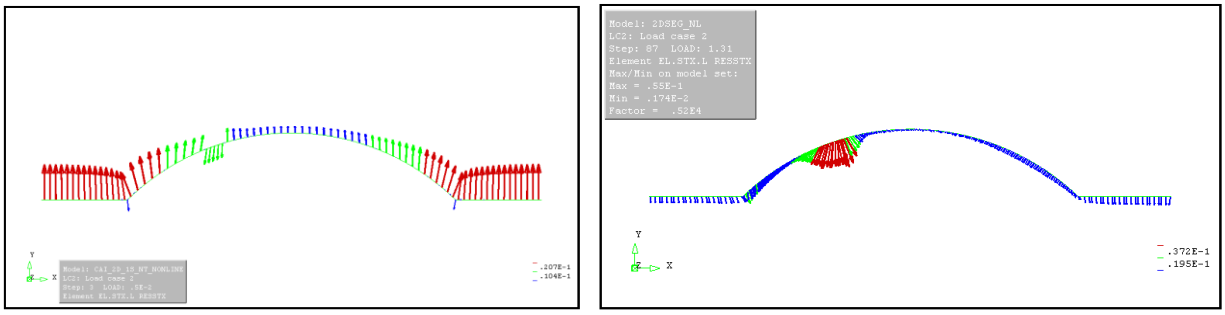

(a) Model A (b) Model 1

Figure 6-7: Interface element normal traction vectors

This improper implementation of interface elements accounts for the differences in results between the two models. A collapse mechanism will occur when four plastic hinges are formed and the plastic hinges are formed when the tensile strength of the masonry is surpassed. In numerical methods, when the interfaces are functioning correctly they reduce large stress in the materials by allowing the two materials to slip thereby relieving internal stresses.

6.2 Finite Element Analysis of Model 2

Model 2 was created to achieve similar results as model B. The lateral edge supports were replaced with a steel wall and ties system to more closely simulate the experiment, with one important modification. Beam elements were used to model the steel wall rather than plane stress elements. This was decided for two reasons

1. Using plane stress elements for the steel wall results in very high element aspect ratios. That is to say, one dimension of the isoparametric element is much larger than the other. This can lead to numerical errors or an unstable solution. Since the steel plate is much deeper and longer than it is wide, its behaviour can be approximated to that of a rectangular beam a uniform cross-section.
2. The other reason beam elements were used is because the beam elements, similar to the steel plate, will add more support to the edge of the bridge. It is assumed that this added support may lead to higher deformations in the arch before collapse, approaching the deformations experienced in the experiment.

Since beam elements were used to model the steel wall, it became necessary to introduce another interface between the steel wall and the edge of the bridge. The nodes of the beam element each have three degrees of freedom and the plane stress elements, two. Therefore, these elements are not compatible with each other without imposing additional constraints. However these constraints would be difficult to implement while trying to maintain realism of the experiment. The solution is to use interface elements. The Interface only feels relative displacements along its normal and tangential

axes (see section 4.1.5). The rotational variables impose additional displacements on the interface but are no longer directly applied to the plane stress elements.

6.2.1 Design process

The design process of Model 2 was similar to model 1. The overall intent was to replicate model B, generated by the previous dissertation. The design process for model two is outlined below.

1. Create preliminary geometry in AutoCAD then import into the FE program.
2. Generate an appropriate mesh and apply relevant element properties.
3. Create sets that will be used in the insertion of interface elements. The sets are listed below:

Table 6-7: Sets related to future interface insertion

Set Name	Description
Ring	All Elements and nodes contained within the surface of the ring
Foot	All elements and nodes contained within the surface of the footings
IFR	All nodes contained on the line where the interface between the ring and fill is to be inserted
Plate	All elements and nodes contained on the line representing the steel wall.
IF_SW	All nodes on the line where the interface between the steel wall and edge of model will be inserted.

4. Generate the data file and import it into a spreadsheet program.
5. Duplicate each node in set IFR and assign it to the 100000s series of new IFR points.
6. Duplicate each node in set IF_SW and assign it to the 200000s series called new IF_SW points.
7. Use the information from the created sets as filters for existing elements.
8. All nodes in the sets FOOT and RING that coincide with the nodes in IFR must be redefined as the nodes in the 100000s series, new IFR nodes.
9. All nodes in the set PLATE that coincide with the nodes in set IF_SW must be redefined as the nodes in the 200000s series, new IF_SW nodes.
10. Introduce new IFR interface elements between the old IFR nodes and the new IFR nodes.
11. In a similar manner, introduce new IF_SW interface elements.
12. Finally the points at which the two interfaces intersection on the model must be modified so two interface elements are not connected to one node. Where ever the nodes of

elements in IF_SW coincide with nodes in IFR, duplicate those nodes with the same coordinates and number them in the 400000s series.

13. Redefine the IF_SW elements to connect to the new 400000s series nodes.
14. Modify the data file and if possible verify the new interface elements with Meshedit. Ensure to modify any sections related the new elements (Materials, geometry...)
15. Run the analysis and verify the responses in the new interface elements.

Issues with this method

In the final steps of the design method, issues arise when it came to reloacating interface elements which were sharing a node. The error was realized when this method was implemented into the 3D model. In step 13, when the IF_SW elements are redefined to the 400000s series, these nodes do not actually connect to anything. The model worked in plane stress because there are only two points of intersection. Conversely, in the 3d model there are lines of intersection and they condition of the stiffness matrix becomes ill-conditioned, then singular.

6.2.2 Geometry

The Geometry of Model 2 is identical to model B except it has five layers of soil rather than three. From Figure 6-8, the different materials are represented by different colours. The steel plates are located on the edges and the steel ties are anchored to each plate to complete the horizontal constraint system.

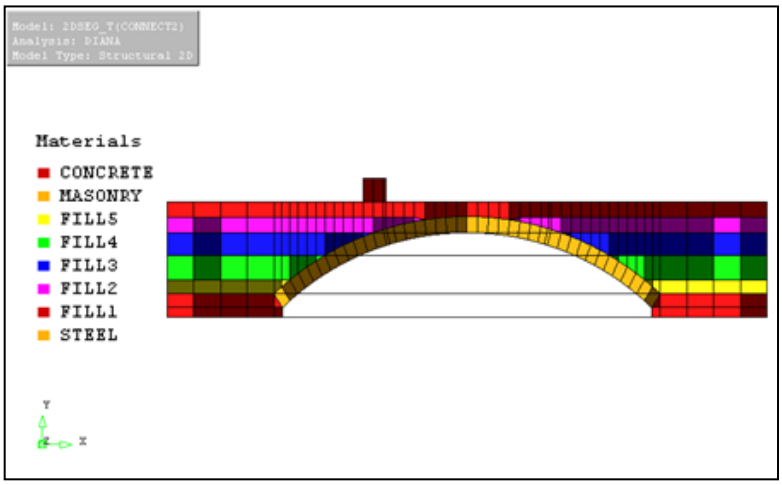

Figure 6-8: Geometry and materials of model 2

6.2.3 Materials

The materials are the same as model 1 except steel has been added for the ties and edge profiles. The properties of steel are written below.

Table 6-8: Steel Material Properties

Property	Value
Young's Modulus [MPa]	200 000
Poisson's Ratio	0.27
Density [kg/m^3]	7 850

6.2.4 Elements

The elements used in this model were as follow (see section 4.1.2)

Material	Element
Concrete	Plane Stress (CQ16M & CT12M)
All infill	Plane Stress (CQ16M & CT12M)
Masonry	Plane Stress (CQ16M & CT12M)
Steel ties	Truss elements (L2TRU)
Steel Plates	Beam elements (L6BEN)

6.2.5 Meshing

The mesh is discretized exactly the same as model 1. The ties have been attached afterwards to the appropriate nodes on the steel plates. Other than at their ends, they do not interact with the rest of the mesh.

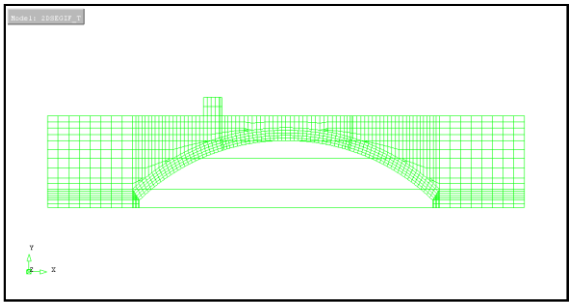

Figure 6-9: Mesh of model 2

6.2.6 Loading Conditions

The loading conditions are the same as model 1. There is also a gravity load applied to all elements.

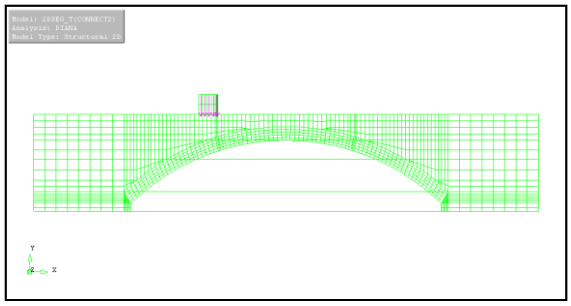

Figure 6-10: Loadings on model 2

6.2.7 Boundary Conditions

The boundary conditions have changed. There is no longer any lateral support as the steel profile and tie system is in place.

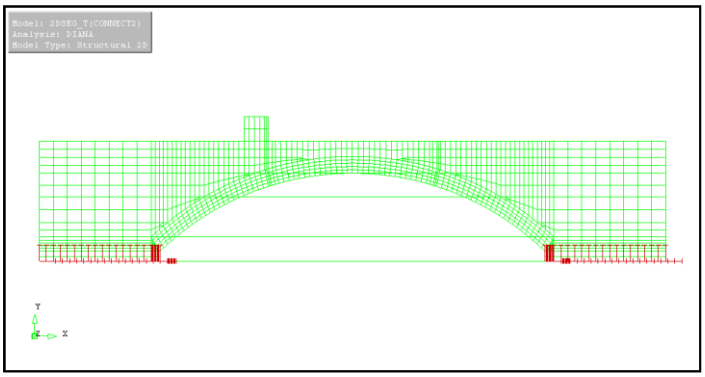

Figure 6-11: Boundary conditions for model 2

6.2.8 Pre-stressing ties

There was an attempt to pre-stress the ties so that they would be loaded before the external load is applied. More compression in the arch will signify a more stable arch and perhaps a more controlled collapse mechanism. However, the pre-stress was not successfully implemented using the FE program.

6.2.9 Linear results

The figure below shows a contour plot of the principle stresses on a deformed shape. The shape is deformed by a factor of 700. The maximum displacement of the ring is 0.36mm.

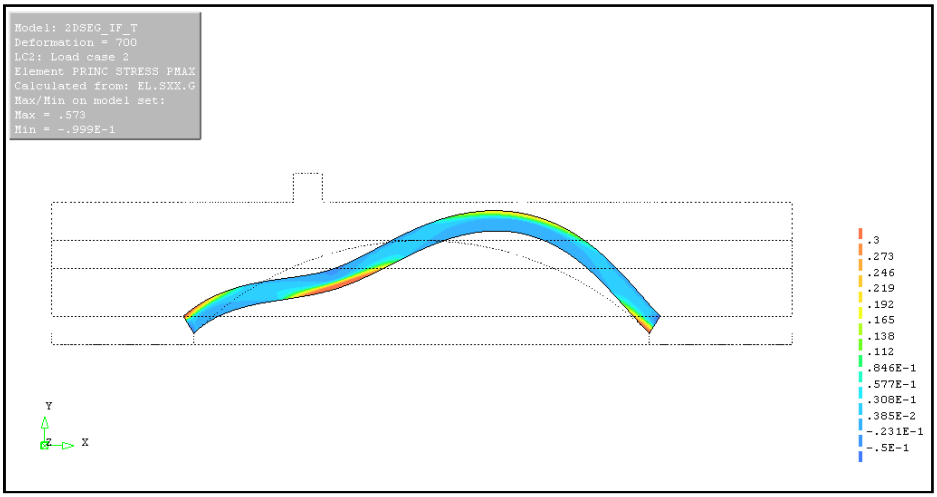

Figure 6-12: Principle stress on deformed ring ($P1_{max}$=0.573, $P1_{min}$ = -0.1 MPa)

Comparison with previous model

The table below is a summary of main attributes which were compared for verification.

Table 6-9: Comparison between model B and model 2

Type of Analysis	Attribute	Model B	Model 1
Linear	Displacement in Ring [mm]	0.296	0.36 [mm]
	Principle stress over entire model [MPa]	0.524	0.573
	Principle stress in ring [MPa]	0.554	0.573

6.2.10 Nonlinear Results

The non linear analysis was conducted using the following parameters:

- Iteration Method: Automatic
- Total Step size: 2
- Max step size: 0.01
- Min step size 0.0001
- Using spherical path arc length method, control node 1163

The model reached an ultimate load of approximately 16KN. This value is similar to that reached by the previous models. The results correlated with what was expected and were comparable to the results obtained in the previous models.

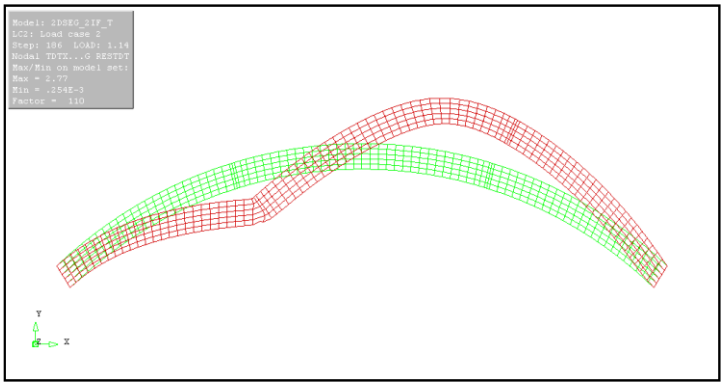

Figure 6-13: Deformation of the ring (Max = 2.77mm)

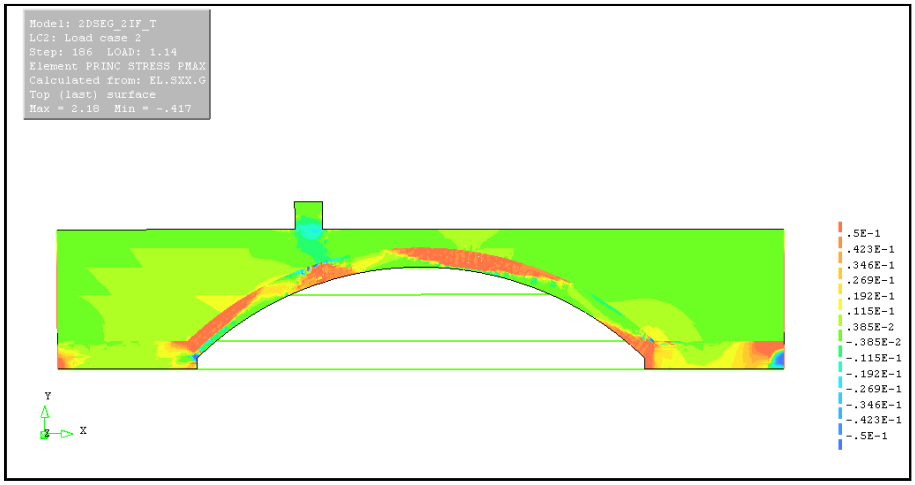

Figure 6-14: Principle stress over entire model ($P1_{max}$ = 2.18, $P1_{min}$=-0.417 MPa)

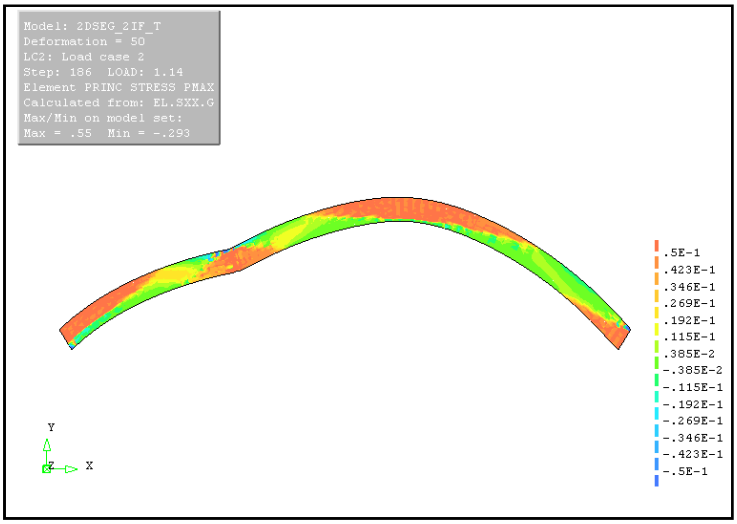

Figure 6-15: Maximum principle stress on deformed ring (P1max=0.55, P1min = -0.293 MPa)

Table 6-10: Comparison of values between model B and model 2

Type of Analysis	Attribute	Model B	Model 1
	Ultimate load reached [KN]	12.9	16
Nonlinear	Displacement in Ring [mm]	0.296	2.77
	Principle stress over entire model [MPa]	2.38	2.18
	Principle stress in ring [MPa]	0.59	0.55

Looking at the result comparisons, the largest difference is when the displacements in the ring are compared. The ring in model 2 has a displacement of 2.77mm where as in model B it experienced 0.296mm of displacement. This can likely be attributed to using beam elements and an interface

rather than plane stress elements. As the structure deforms, it is still constrained by the steel walls on either edge, and this allows larger deflections before failure.

6.2.11 Comparison with experimental results

The data from the extensometers from the test were compared to the displacements in model 2. The next figures show the results from the experiment (a) and the results from model 2 (b).

(a)

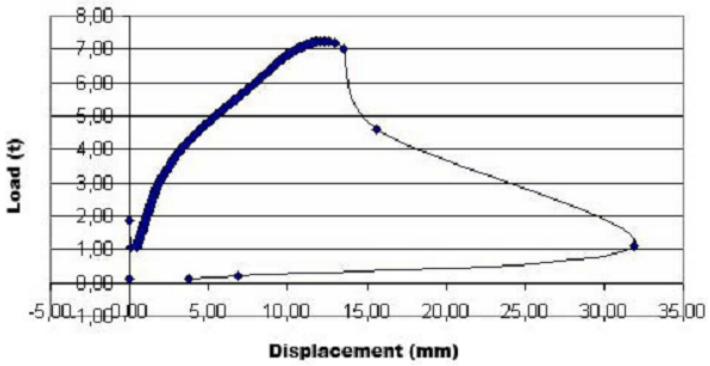

(b)

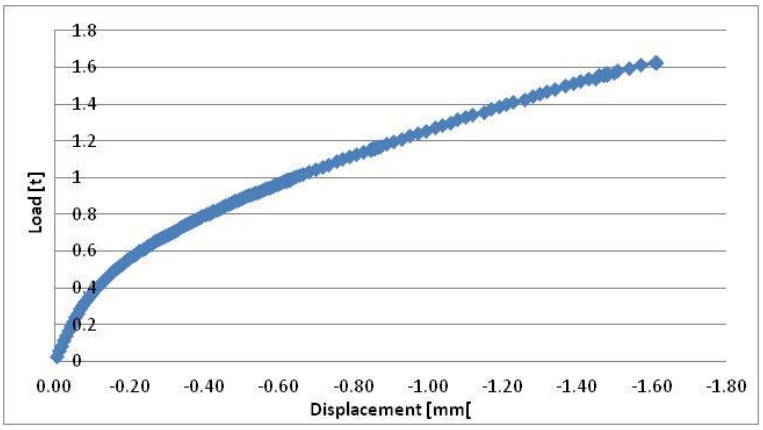

Figure 6-16: Displacements under point of loading

(a)

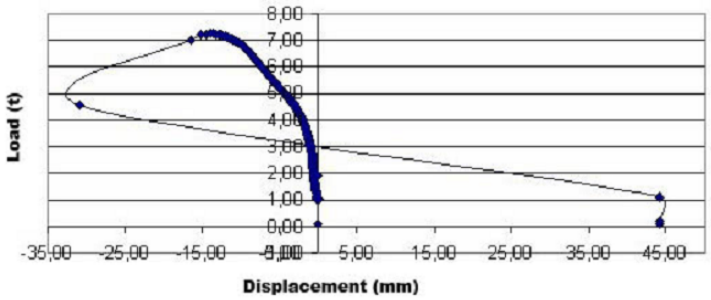

(b)

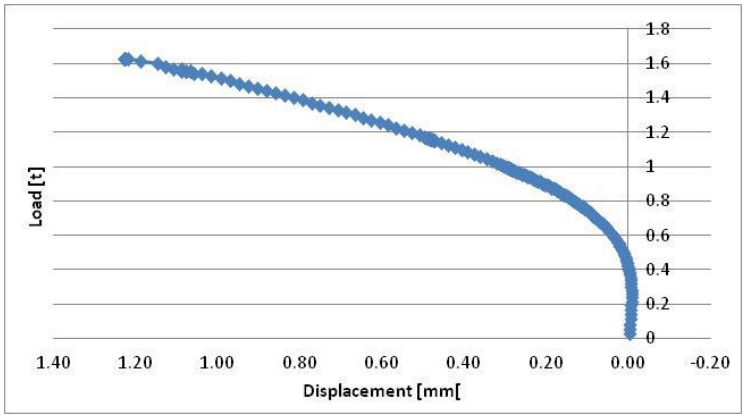

Figure 6-17: Displacement at center of ring

(a)

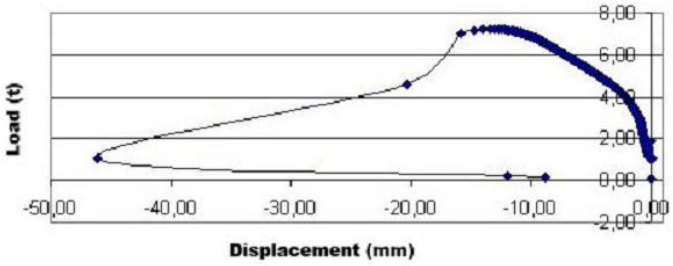

(b)

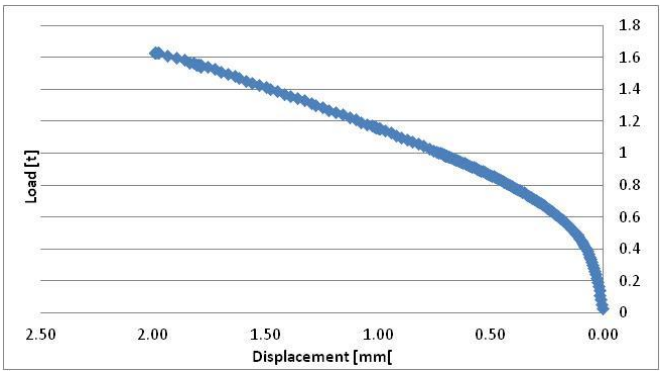

Figure 6-18: Displacement at point symmetrical to load

The three graphs from model 2, although different in magnitude, seem to follow a similar to pattern to the results from the extensometers in the experiment. The slope is consistently less steep in the

graphs from model 2. There are also small plateaus before unloading in the experiment graphs and these were not simulated with model 2. These discrepancies can be an indicator to the difference between modelling a 3D structure using plane stress elements. As an example, the contribution of the spandrel walls will make a stiffer structure.

6.3 Finite Element Analysis of Model 3

Once the analyses for the plane stress models were completed and verified. The next phase was to construct a 3D model. An important aspect of the 3D model was the additional contribution of the spandrel walls.

6.3.1 Design process

Model 3 was generated in a similar manner as model 2. Having an added dimension simply means points becomes lines, lines become planes and surfaces become bodies. One significant difference was the implementation of the interfaces. In three dimensions, the interface lines become planes and as a result, in this model there are three intersection planes. Since perpendicular interfaces could not share the same node, it was necessary come up with a way for the interfaces to share the coinciding lines of intersection. This “mesh stitching” will be discussed in detail in this section. Following this are the design steps involved in generating model 3.

1. Create preliminary geometry in AutoCAD then import into the FE program.
2. Generate an appropriate mesh and apply relevant element properties.
3. Create sets that will be used in the insertion of interface elements. The sets are listed below:

Set Name	Description
Ring	All Elements and nodes contained within the body of the ring
Foot	All elements and nodes contained within the body of the footings
IFR	All nodes contained on the plane where the interface between the ring and fill is to be inserted
Plate	All elements and nodes contained on the plane representing the steel wall.
IF_SW	All nodes on the plane where the interface between the steel wall and edge of model will be inserted.

4. Generate the data file and import it into a spreadsheet program.
5. Duplicate each node in set IFR and assign it to the 100000s series of new IFR points.

6. Duplicate each node in set IF_SW and assign it to the 200000s series called new IF_SW points.
7. Use the information from the created sets as filters for existing elements.
8. All nodes in the sets FOOT and RING that coincide with the nodes in IFR must be redefined as the nodes in the 100000s series, new IFR nodes.
9. All nodes in the set PLATE that coincide with the nodes in set IF_SW must be redefined as the nodes in the 200000s series, new IF_SW nodes.
10. Introduce new IFR interface elements between the old IFR nodes and the new IFR nodes.
11. In a similar manner, introduce new IF_SW interface elements.
12. For model 3, there were no steel plates or ties in the geometry model. However, the new steel plate elements will coincide with the if_SW elements. The steel elements will be formed by the new side of the if_SW elements (30000s series)

6.3.2 Weaving the Mesh

The locations where two interfaces intersect on the model must be modified so two perpendicular interface elements are not connected to one node. In model 3 this occurs at on three different lines. The figure below shows the outline of model 3 with all three of the interfaces and their intersection locations visible.

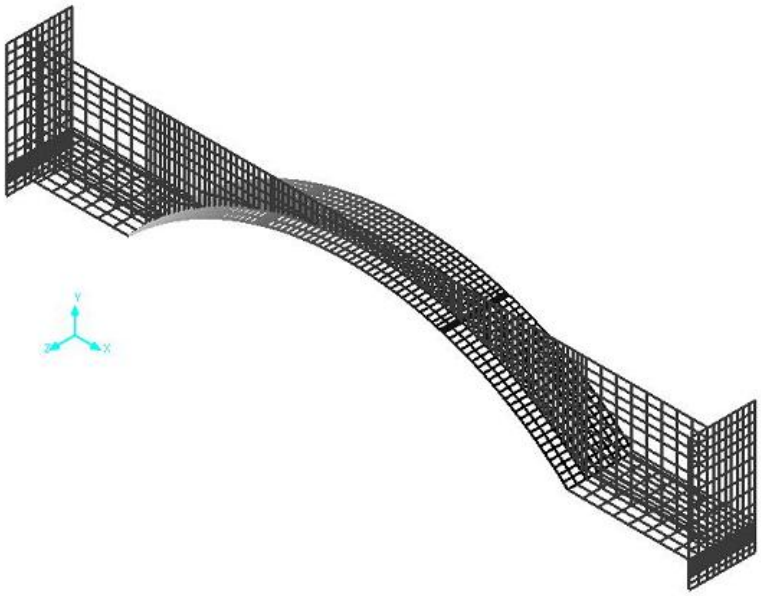

Figure 6-19: View of three intersection interface planes

In order to overcome this issue, the perpendicular interfaces are essentially “woven” together. All of the quadrilateral elements in contact with the line of intersection become triangular then the vertices of each triangular element are connected to every second node on the line. The other plane is connected

to the remaining nodes. Recalling from section 4.1.2, a triangular plane stress element is a quadrilateral element with one end collapsed into one node. This results in constant strain over the element rather linear varying strain. This is similar to what happens with an interface element. At the locations of intersection, rather than the relative displacements being integrated linearly over the element, they produce constant values. This is a drawback to the mesh weaving technique. However, this error can be reduced by reducing the area of the elements with any refinement technique. The result of weaving the mesh is shown below.

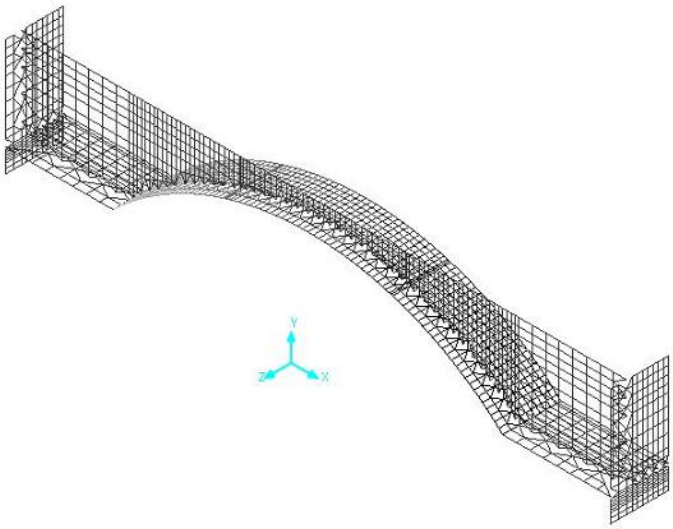

Figure 6-20: Result after weaving mesh

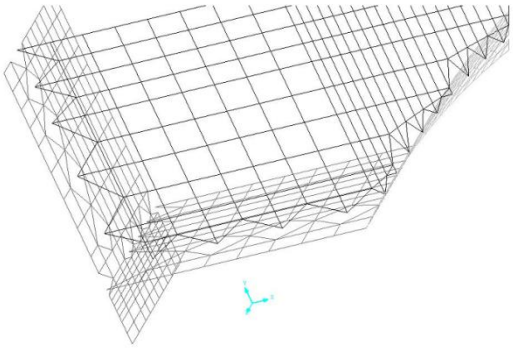

Figure 6-21: Detail of mesh weaving

In Figure 6-20 and Figure 6-21, it can be seen that there are no longer any common nodes between the intersection planes. All the original geometry of the bridge remains unaffected.

Linear Results

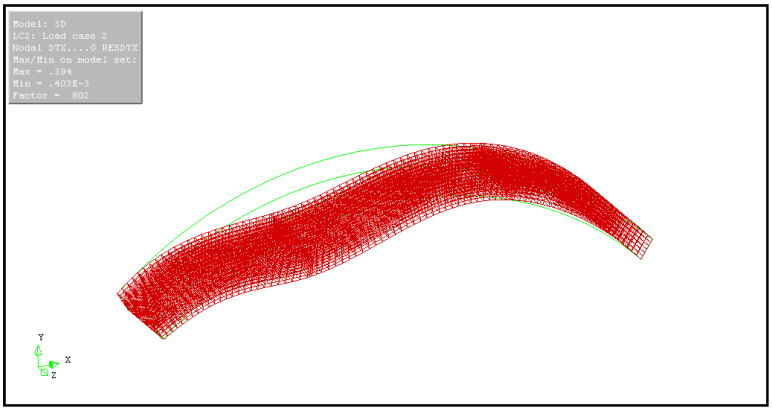

Figure 6-22: displacement result on ring (max = 0.394 mm)

(a) Max = 8.17 MPa

Min = -0.465 MPa

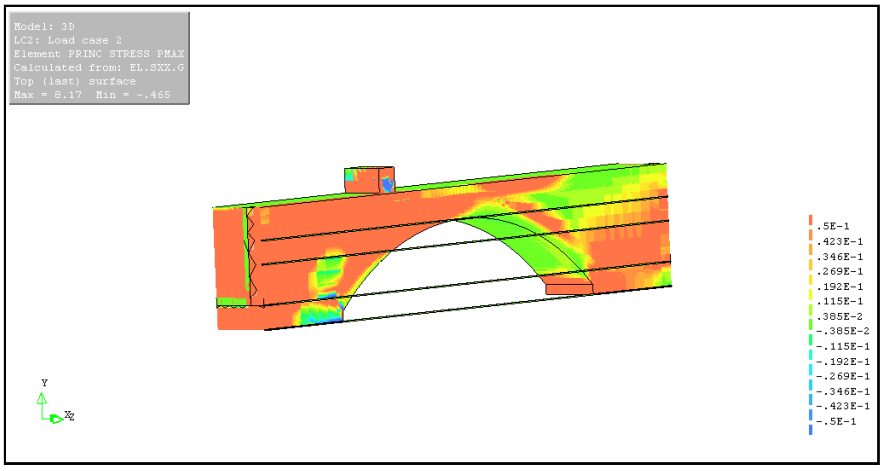

(b) Max = 0.803

Min = -0.201

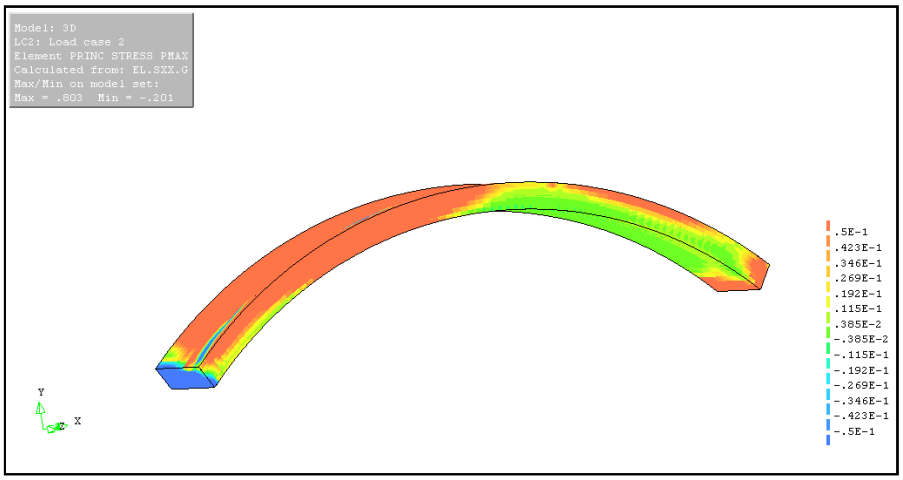

Figure 6-23: Principle Stress result over entire model (a) and only the ring (b)

Linear Results Discussion

The linear results do not show what was expected of this model. There is a significant increase in stresses all over the model and the mechanism of the ring has changed as well. This isn't necessarily due to the interfaces because in a linear analysis, the interfaces have no affect on the structure. Interfaces are only functioning when materials are slipping. The system is being loaded incorrectly or perhaps the arch is being supported incorrectly.

Nonlinear Results

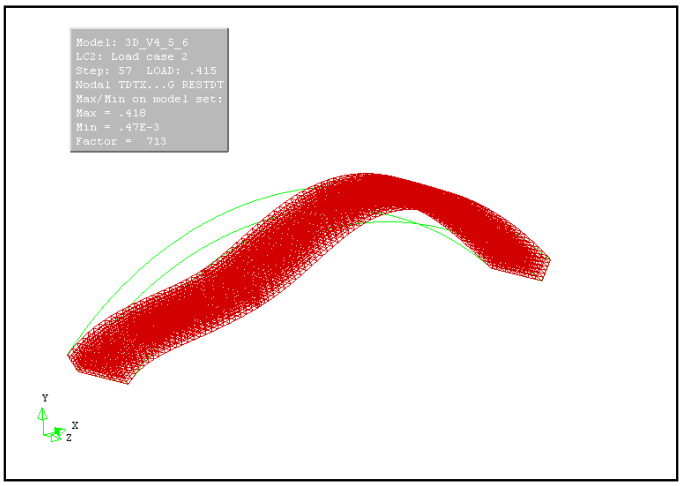

Figure 6-24: Deformation in ring (max=0.418mm)

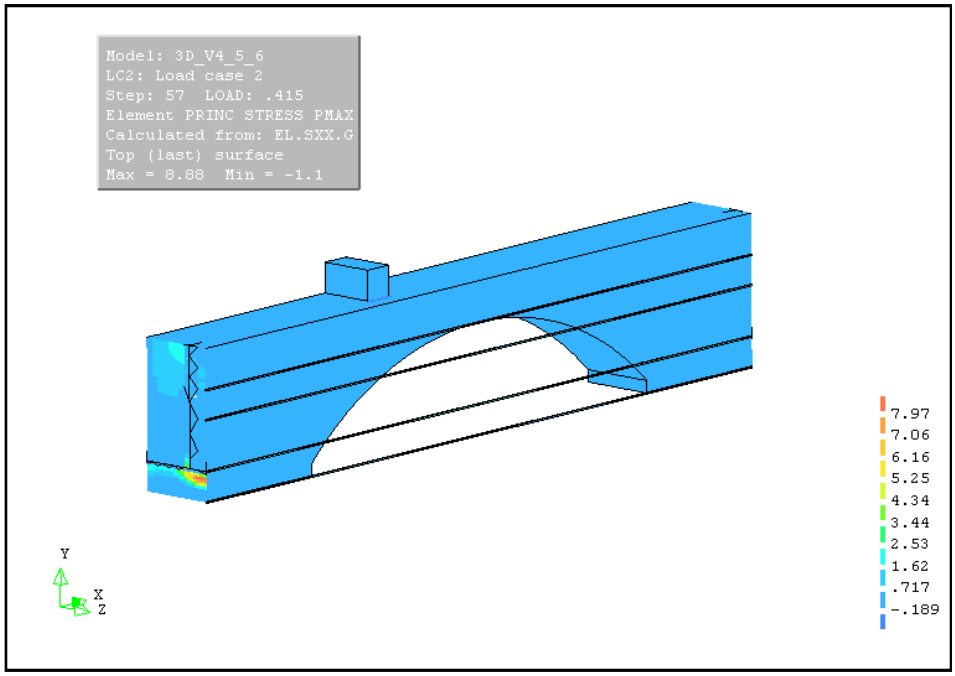

Figure 6-25: Principle stress over entire model($P1_{max}$=8.8, $P1_{min}$=-1.1 MPa)

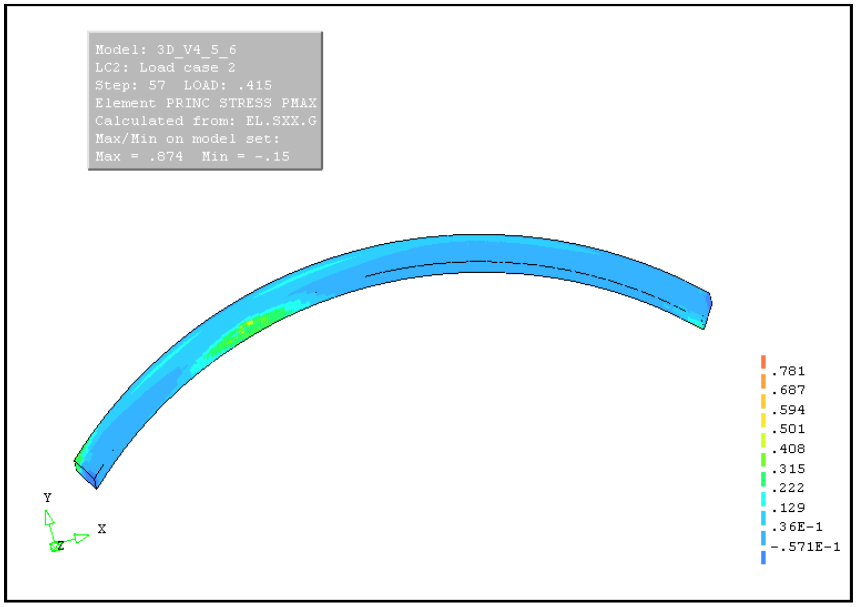

Figure 6-26: Principle stress in the ring($P1_{max}$=0.874,$P1_{min}$=-0.15 MPa)

Discussion on nonlinear results

As would be expected from the linear analysis results, the nonlinear behaviour of model three does not correlate with the expected behaviour. The maximum deformation in the masonry ring is 0.418mm and the max deformation in ring in model 2, the plane stress model reached 2.77mm. This is an indication that the spandrel walls are making the structure stiffer, and therefore experiencing less displacement. When the stress results are observed, the large stresses and the lack of development of the four hinges in the arch ring are indications that the model is not functioning correctly. In this 3D model there are a multitude of parameters which significantly influence the behaviour of the arch during analysis. In order to achieve convergence with this model it was necessary to increase the masonry properties. This was to be the beginning of a trial and error analysis to achieve convergence but due to lack of time, this analysis will have to be passed on for continued analysis.

Discussion on the interface implementation technique

The interface insertion technique applied to these models was successful. Once the framework of the spreadsheets was set up, the addition of interfaces came relatively easy. However, at times the incorporation of interfaces involved tedious spreadsheet manipulation and careful consideration had to be made that the orientation of the elements were correct. The actions performed in the spreadsheet are very basic and to someone with more programming knowledge, it can be the framework for an interface implementation program. The key concept with this program is it uses only existing geometry to incorporate the interfaces. Theoretically, this method can be applied to almost any model. The

challenge will arise when the geometry of the model becomes more complex. It is much easier to implement quadrilateral and triangular elements in a spreadsheet, then curved elements.

7. CONCLUSION

The objectives of the dissertation were to successfully model the experiment conducted in 2001 using 3D finite element analysis. At first previous models were provided. These models were to be used for continued analysis however after being put through a verification process. The results achieved in the previous dissertation were not able to be replicated. Therefore new models were generated. A detailed explanation of the design process for the new bridge models was discussed. In the design process, the method by which interfaces were incorporated into the models was explained. The method used a spreadsheet program to manipulate the data file generated by the FE program to create the interface elements. The method proved to be tedious work and it was possible to overlook an error while creating the new elements. However, the method serves as a framework to be used for the design of a potential interface insertion program. The results of model 1 were different than those of the model A. This was attributed to the inconsistency of the element local axes. It can be concluded that the proper functioning of interface elements leads to higher ultimate load factor being reached before collapse. The results of model 2 were most conclusive. The displacements at the same location of the extensometers in the experiment seemed to correlate well with the data from the experiment. This plane stress model was a reasonable approximation to the experiment.

Generation of the 3D model yielded unexpected results. Neither the stress nor the displacements correlated with those of any of the previous models. It seems the ring is being loaded differently as there is no indication of the formation of hinges in the four expected locations on the ring.

7.1 Suggestions for further study

- The 3D model should be reinvestigated to determine the reason for the abstract behaviour compared to its predecessors.
- It would be interesting to see how the structural response differs with the ties being pre-stressed before the load is applied
- If possible, it would be interesting to see the frame work of implementing interfaces incorporated into an automated program.
- Once a functioning 3D model is in place, a parametric study would be interesting and may approach more realistic results as those obtained in the experiment.
- Finally, during the loading process in the experiment, the footings experienced a significant rotation, thus altering the collapse mechanism of the bridge. This could be a possible subject for analysis.

8. REFERENCES

Cai, Y. (2012). "Detailed numerical stimulation of experiments on masonry arch bridge using 3D FE."

Diana, T. (2009). Element Library. Delft, The Netherlands.

Kabele, P. (2011). SA2.6: Structural Analysis Techniques - Finite Element Method III - Practice. SA2 Lecture Slides, Structural Analysis of monuments and Historical Constructions.

Kabele, P. (2012). Structural Analysis Techniques - Finite Element Method II. SA2 Lecture slides.

Pere Roca, A. O. (2011). SA1.09 Ancient Rules and Classical Approaches. Part 1. SA 1 Lecture Slides, University do Minho.

Serna, J. (2001). Caracterizacíon experimental del comportamiento hasta rotura de puentes en arco de obra de fábrica. UPC.

Tech, M. "Modeling errors and Accuracy." Retrieved July, 2012, from http://www.me.mtu.edu/~bettig/MEEM4405/Lecture10.pdf.

Thai, N. C., et al. Automatic Mesh Generation of Joint/interface Elements. ICCM12.